# Summary of Large-Scale Nonplanar Reinforced Concrete Wall Tests

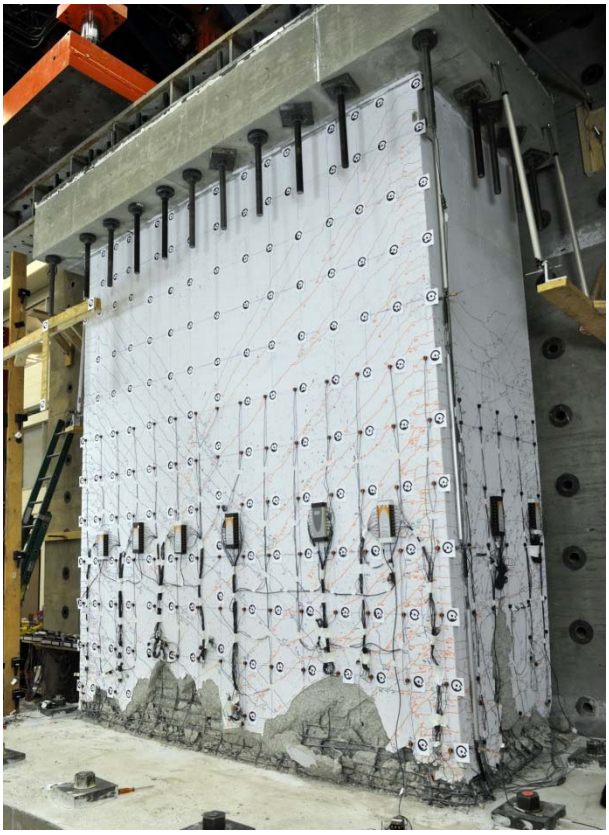

Anahid Behrouzi, Tufts University
Andrew Mock, SCA Consulting Engineers
Dr. Laura Lowes, University of Washington
Dr. Dawn Lehman, University of Washington
Dr. Daniel Kuchma, Tufts University

Funding provided by the **National Science Foundation** and the **Charles Pankow Foundation**

# Behavior of Nonplanar Reinforced Concrete Walls

**Anahid Behrouzi, University of Illinois**
**Andrew Mock, SCA Consulting Engineers**
**Dan Kuchma, Tufts University,**
**Laura Lowes and Dawn Lehman, University of Washington**

## 1 INTRODUCTION

Nonplanar wall configurations are prevalent in engineering practice, yet relatively little research has addressed nonplanar walls and the earthquake response of these components remains poorly understood. A recent experimental test program conducted by the authors investigated the earthquake response of modern, ACI Code compliant C-shaped walls subjected to unidirectional and bidirectional lateral loading. To compare the results of this study with previous experimental investigations conducted by others, this document examines laboratory tests of slender nonplanar walls available in the literature. Response histories, damage patterns, drift capacity and failure mechanisms are used to characterize the behavior of each nonplanar wall test specimen. The impact on behavior of various design parameters as well as unidirectional versus bidirectional load history is investigated. Results are synthesized to provide improved understanding of behavior and guidance for design of nonplanar walls.

Section 2 provides an overview of the nonplanar wall test found in the literature. Section 3 provides a more in-depth overview of C- and U-shaped walls, including the C-shaped wall tests conducted as part of this study. Section 4 presents failure and response mechanism observed during nonplanar wall tests. Section 5 summarizes observations and presents conclusions about nonplanar wall behavior.

## 2 NONPLANAR WALLS TEST PROGRAMS

To improve understanding of behavior, previous experimental tests of nonplanar walls were reviewed. Eleven test programs comprising 28 test specimens were found in the literature. Wall specimens had C, U, H, L and T-shaped configurations; all specimens had one axis of symmetry. All specimens were subjected to cyclic lateral loading with a shear span ratio (ratio of effective height of the applied base shear to in-plan length of the wall) greater than 2.0; all specimens exhibited predominately flexure-controlled behavior. Some specimens were subjected to axial loading; some specimens were subjected to bidirectional lateral loading, using a cruciform, clover leaf, or other lateral displacement path. Table 1 provides basic information for the test specimens reviewed, and Table 2 provides details of specimen compliance with ACI 318-14 Code requirements for detailing of special boundary elements. Sections 2.1 through 2.10 review the test programs, including research objectives, tests parameters, and primary observations and conclusions. Section 2.11 provides overarching observations and conclusions about nonplanar wall behavior.

**Table 1: Nonplanar wall test programs and specimens**

| Test Program Reference | Specimen ID | Wall Shape | Lateral Loading | |
|---|---|---|---|---|
| | | | Unidirectional | Bidirectional |
| Lowes et al (2014) | CW1 | C | SA | |
| | CW2 | C | | SA,WA |
| | CW3 | C | | SA,WA |
| Ile & Reynouard (2005) | IleX | U | SA | |
| | IleY | U | WA | |
| | IleXY | U | | CL |
| Beyer et al (2008) | TUA | U | | SA,WA, 45and CL |
| | TUB | U | | SA,WA,45 and CL |
| Oesterle (1976/1979) | F1 | H | SA | |
| | F2 | H | SA | |
| Paulay & Goodsir (1985) | Wall 3 | T | SA | |
| Thomsen & Wallace (1995) | TW1 | T | SA | |
| | TW2 | T | SA | |
| Brueggen (2009) | NTW1 | T | | SA,WA and 360 sweep? |
| | NTW2 | T | | SA,WA and 360 sweep |
| Inada et al. (2008) | L00A | L | PL | |
| | L45A | L | 45 | |
| | L45B | L | 45 | |
| Kono et al. (2011) | L45C | L | 45 | |
| | L45D | L | 45 | |
| Hosaka et al. (2008) | L-1 | L | 45 | |
| | L-2 | L | 45 | |
| | L-5 | L | 45 | |
| | L-6 | L | 45 | |
| Li (2010) | DL1 | L | PL | |
| | DL2 | L | PL | |
| | DL3 | L | PL | |
| | DL4 | L | PL | |

Note: SA = Strong axis loading, WA = Weak axis loading, CL = cloverleaf or similar bidirectional load pattern, PL = Loading parallel to leg, 45 = Loading 45° to leg, 360 sweep = approximately circular lateral displacement path possibly with radius varying with angle.

**Table 2: Evaluation of specimen compliance with ACI 318-14 Code requirements for special boundary elements**

| Researcher | Spec. | $b_{e,min}$ | $b_{min}$ | $h_{x,max}$ | $s_{max}$ | $A_{sh,min}$ | Crosstie Hook Ext. | ACI 318-14 Compliant |
|---|---|---|---|---|---|---|---|---|
| | | $max\begin{cases} c-0.1\ell_w \\ c/2 \end{cases}$ | $max\begin{cases} h_u/16 \\ 12\ in. \end{cases}$ | $min\begin{cases} 2b/3 \\ 14\ in. \end{cases}$ | $min\begin{cases} b/3 \\ 6d_b \\ 4'' < 4+\frac{14-h_x}{3} < 6'' \end{cases}$ | $max\begin{cases} 0.3sb_c\left(\frac{A_g}{A_{ch}}-1\right)f_c'/f_{yt} \\ \frac{0.09sb_c f_c'}{f_{yt}} \end{cases}$ | $max\begin{cases} 6d_b \\ 2\ in. \end{cases}$ | |
| **Beyer et al.** | TUA | YES | YES | YES | YES | $\frac{A_{sh}}{sb_c}=0.01<0.09\frac{f_c'}{f_{yt}}=0.014$ | YES | NO |
| | TUB | YES | YES | $h_x=3.9>2b/3=2.6$ | $s=2.0>b/3=1.3$ | YES | YES | NO |
| **Ile & Reynourd** | IleX | YES | YES | YES | $s=3.54>\frac{b}{3}=3.3$ | YES | NA | NO |
| | IleY | YES | YES | YES | | YES | NA | NO |
| | IleXY | YES | YES | YES | | YES | NA | NO |
| **Lowes et al.** | CW6 | YES | YES | YES | $s=2.25>b/3=2.0$ | YES | YES | NO |
| | CW7 | YES | YES | YES | | YES | YES | NO |
| | CW8 | YES | YES | YES | | YES | YES | NO |
| **Bruggen** | NTW1 | YES | YES | YES | YES | YES | YES | YES |
| | NTW2 | YES | YES | YES | YES | YES | YES | YES |
| **Oesterle et al. *** | F1 | | - | - | - | - | - | - |
| | F2 | YES | YES | YES | YES | $\frac{A_{sh}}{sb_c}=0.007<0.09\frac{f_c}{f_{yt}}=0.01$ | NA | NO |
| **Thomson & Wallace** | TW1 | YES | YES | YES | $s=3.0>b/3=1.3$ | $\frac{A_{sh}}{sb_c}=0.006<0.09\frac{f_c}{f_{yt}}=0.01$ | NA | NO |
| | TW2 | YES | YES | YES | YES | YES | NA | YES |
| **Inada** | L00A | YES | YES | YES | YES | $\frac{A_{sh}}{sb_c}=0.007<0.3(\frac{A_g}{A_{ch}}-1)\frac{f_c'}{f_{yt}}=0.026$ | NA | NO |
| | L45A | | - | YES | YES | | NA | NO |
| **Kono** | L45C | | - | YES | $s=2.4>b/3=1.6$ | $\frac{A_{sh}}{sb_c}=0.006<0.3(\frac{A_g}{A_{ch}}-1)\frac{f_c'}{f_{yt}}s=0.021$ | NA | NO |
| | L45D | | - | YES | | | NA | NO |
| **Funaki** | L1 | | - | YES | $s=1.6>6d_b=0.9$ | $\frac{A_{sh}}{sb_c}=0.002<0.3(\frac{A_g}{A_{ch}}-1)\frac{f_c'}{f_{yt}}=0.018$ | NA | NO |
| | L2 | | - | YES | $s=1.2>6d_b=0.9$ | | NA | NO |
| | L5 | | - | YES | $s=1.6>6d_b=0.9$ | $\frac{A_{sh}}{sb_c}=0.005<0.3(\frac{A_g}{A_{ch}}-1)\frac{f_c'}{f_{yt}}=0.015$ | NA | NO |
| | L6 | | - | YES | | | NA | NO |
| **Li** | DL1- | YES | $b=3.9<\frac{12}{scale}=6$ | YES | YES | YES | NA | NO |
| | DL2- | YES | | YES | $s=2.4>b/3=1.3$ | YES | NA | NO |
| | DL3- | YES | | YES | YES | YES | NA | NO |
| | DL4- | YES | | YES | $s=2.4>b/3=1.3$ | YES | NA | NO |

Notes: "NA" indicates data were not available to check requirement. "-" indicates requirement is not applicable. *special boundary elements not required for walls by Oesterle et al. Requirements including absolute limits (e.g., $b_{max}$ > 12in.) were evaluated using the absolute limit divided by specimen scale ($scale = wall\ thickness/12\ in. < 1.0$).

## 2.1 Lowes et al. (2014): C-shaped Wall Tests

A series of three nominally identical C-shaped walls were tested as a part of a research collaboration between the University of Washington and the University of Illinois at Urbana-Champaign. The tests investigated the earthquake performance of modern, ACI Code-compliant slender walls. The overarching objective of the research program was to develop recommendations for performance-based seismic design of reinforced concrete walls with complex geometries, and both experimental testing and numerical modeling were used to investigate wall behavior and advance wall design.

The C-shaped wall test specimens represent the bottom three stories of a 10-story prototype building, and are considered 1:3 scale models by the research team. Wall specimen design was based on data collected from a West Coast building inventory and input from an external advisory panel comprising structural engineers from Magnusson Klemencic Associates and KPFF in Seattle. Specimen design adhered to the specifications of ACI 318-05 and ASCE-7 2005. The specimen configuration is referred to as "C-shaped" as flange length is significantly shorter than web length (ratio of flange to web length is 0.4). The three test specimens are nominally identical in terms of geometry, reinforcement layout, and material properties. All specimens had well-confined boundary elements with heavy longitudinal reinforcement located at the toes of the flanges and the corners of the wall; interior regions of the walls, between the boundary elements, were lightly reinforced (horizontally and vertically). The primary parameter that varied between tests was loading. The first wall (CW1) was subjected to unidirectional cyclic lateral loading in the X-direction (parallel to the web activating strong axis bending) with a constant axial load of $0.05f_cA_g$. The second test (CW2) followed a bidirectional cruciform pattern in the X- and Y- directions (parallel and perpendicular to the web activating strong and weak axes) also with a constant axial load of $0.05f_cA_g$. During cycling to +/-1% drift in the X-direction (strong axis) and +2.25%/-1.1% drift in the Y-direction (weak axis), maximum drift capacity of the loading apparatus was reached and strength loss was not observed; thus, during subsequent loading cycles, the specimen was subjected to true bi-directional loading with displacement in the Y-direction (weak axis) held constant near loading apparatus maxima (+2% and -1.1%) while the specimen was subjected to displacement cycles, with increasing maximum displacement demands, in the X-direction. The third test (CW3) simulated loading of a C-shaped wall in a coupled wall system; the wall was subjected to a cruciform lateral displacement history with the axial load held constant at $0.05f_cA_g$ for loading in the X-direction (strong axis) and with the axial load varied between tension and compression for loading in the Y-direction (weak axis). For the third test, numerical simulation of the 10-story core wall system was employed to define the load history employed in the laboratory (Lowes et al. 2014).

For each of the C-shaped wall tests, loss of lateral load carrying capacity resulted from buckling-rupture failure of longitudinal bars. Typically, significant strength loss occurred when corner boundary element bars fractured. Additionally, for all of the test specimens, it was observed that prior to significant strength loss, nearly all of the vertical reinforcement outside of the boundary elements in both the web and flange regions ruptured at the wall-footing interface. Rupture of vertical reinforcement led to sliding at the wall-foundation interface during subsequent X-direction (strong axis) displacement cycles. This sliding represented a considerable fraction of the total wall displacement and resulted in out-of-plane bending of flanges, dowel action of boundary element reinforcement, and separation of corner boundary elements from the web. For all of the specimens, damage progression was essentially the same; however, specific damage states occur at very different drift demands. The flexural strength of the three walls was approximately the same, and the backbone curve for strong axis flexural behavior was essentially identical until maximum strength was achieved. For loading beyond maximum strength in the X-direction (strong axis), weak-axis loading affected response, reducing drift capacity and unloading-reloading stiffness.

## 2.2 Ile & Reynouard (2005), Reynouard and Fardis (2001) and Pegón et al. (2000): U-shaped Wall Tests

Three U-Shaped walls were designed and analyzed by Reynouard and Fardis (2001) and tested under quasi-static cyclic loading by Pegón et al. (2000) at the European Laboratory for Structural Assessment (ELSA). The objectives of the study were to improve understanding of the earthquake response of nonplanar walls, refine numerical modelling approaches used for nonplanar walls subject to combined loading, and provide recommendations for design.

Each of the three U-Shaped walls had the same cross-section geometry and reinforcement layout and was designed in accordance with ENV1998-1-3:1994 and the proposed revision in prEN19888-1: 2001. The walls are described as U-shaped as the ratio of flange length to web length (ratio = 0.83) is substantially larger than for the C-shaped walls (ratio = 0.4) tested by Lowes et al. (2014). The three nominally identical wall specimens were subjected to different lateral displacement histories. The first two wall tests were each subject to a unidirectional cyclic lateral loading protocol: Wall 1 was tested in the X-direction (parallel to the web of the wall activating strong axis bending) and Wall 2 in the Y-direction (perpendicular to the web of the wall activating weak axis bending). The third test examined the effects of bi-directional loading by employing a butterfly loading pattern with both X and Y components.

The primary conclusions of the experimental test program were that in comparison with unidirectional loading, bidirectional loading results in reduced drift capacity in both strong- and weak-axis loading directions as well as more rapid strength loss. Additionally, researchers concluded that under bidirectional loading, shear forces due to Y-direction (weak-axis) bending are resisted primarily by the wall flange that carries compression due to X-direction (strong-axis) bending; as such, they recommended that each wall flange be designed to carry the entire shear demand on the wall. Finally, the researchers concluded that the experimental results suggest the adequacy of critical region confinement included in prEN19888-1:2001.

## 2.3 Beyer et al. (2008): U-shaped Wall Tests

Two U-shaped walls were tested at ETH Zurich to build on the Ile and Reynouard (2005) study and provide further understanding of i) the vulnerability of U-shaped walls to shear and sliding shear mechanisms, ii) the effects of load direction on stiffness, strength, and deformation capacity, and iii) the contributions of flexural, shear, and sliding deformations to total wall deformation. The primary test parameter was wall thickness, as wall thickness was expected to have a significant impact on shear response mechanisms observed by Ile and Reynouard. Specimens were not designed to meet the requirements of a particular design code, but were detailed to achieve high ductility without being overly conservative in terms of shear and sliding shear strength; both specimens were designed with concrete shear keys at the wall-foundation interface to resist sliding shear. The walls were subjected to identical loading histories that included, at increasing ductility demand levels, a cruciform pattern inducing strong- and weak-axis bending independently, a diagonal load cycle inducing strong- and weak-axis bending simultaneously, and a bi-directional "sweep" inducing strong- and weak-axis bending. Walls were subjected to a constant axial load. The same total load was applied to each specimen, this represented an axial load of $0.02f_cA_g$ for TUA and $0.04f_cA_g$ for TUB.

Test results support several important conclusions about nonplanar wall behavior. First, despite detailing intended to achieve ductile response, the thinner wall exhibited a compression failure; this was attributed to severe spalling of boundary element concrete under bidirectional loading and, as a result, significant loss of cross-sectional area and reduced compressive capacity. The researchers noted that

this is particularly troubling as wall response under bidirectional loading may not be considered due to limitations of design and analysis software. Second, it was observed that shear deformation in nonplanar walls depends on the direction of loading and can significantly exceed that observed in planar walls, such that special provisions may be required for design of nonplanar walls.

## 2.4 Oesterle (1976, 1979): H-shaped Wall Tests

Two H-shaped walls were tested by researchers at the Portland Cement Association to improve understanding of the earthquake behavior of walls. The primary test parameters were the amount of flexural reinforcement, presence of confinement in the boundary elements, and application of axial load. The first H-shaped wall had a longitudinal reinforcement ratio of 3.89% and was not subjected to axial load; the second H-shaped wall had a slightly larger reinforcement ratio of 4.35% and was subjected to an axial load of $0.07f_cA_g$. Both walls were subjected to high shear demand-capacity ratios ($V_{max}/V_n$ = 1.02 and 1.19). The flanges in the first wall were considered boundary elements and detailed as compression columns; the second wall had confined boundary elements at the web-flange intersection only. The design moment of both walls was calculated using the 1971 ACI Code and horizontal reinforcement was provided to meet the shear demand associated with this moment.

For both specimens, loss of lateral load carrying capacity resulted from crushing of unconfined web concrete adjacent to the web-flange boundary element. The research team attributed this to high shear stress demand and the development of a relatively small and highly stressed compression zone at the web-flange intersection. The loss in load capacity was both rapid and significant. Boundary element confining reinforcement was observed to delay crushing failure by delaying bar buckling and maintaining core concrete strength. Additionally, it was observed that shear deformation in the plastic hinge region of the wall were a significant portion of the total deformation.

## 2.5 Paulay & Goodsir (1985): T-shaped Wall Test

One T-shaped wall was tested at the University of Canterbury. The test was part of a larger research program addressing two major gaps in technical knowledge identified during drafting of the NZS 3101:1982 document that provides guidelines for the seismic design of ductile structural walls. These gaps in knowledge were (1) whether existing provisions were sufficient to prevent inelastic instability of thin walls and (2) how to design and detail transverse reinforcement to provide adequate confinement of wall compression zones. Secondary objectives of the test was to develop a better understanding of the load-deformation response of thin-walled sections and associated failure mechanisms when subjected to reversed cyclic loading.

The T-shaped wall was subjected unidirectional cyclic lateral loading parallel to the stem of the wall. To investigate inelastic instability, a varying axial load ($0.02\text{-}0.12A_gf_c$) was applied that resulted in large compression demands on the tip of the stem. Heavy confining reinforcement was provided over approximately 90% of the computed compression region in the tip of the stem; whereas lighter confining reinforcement (more widely spaced than in the stem and designed only to delay onset of bar buckling only) was provided in the tips of the flange.

The T-shaped wall failed due to crushing of confined concrete in the boundary element at the tip of the stem and adjacent unconfined concrete. Lateral instability was deemed indirectly responsible for this mechanism, as the stem of the specimen experienced significant out-of-plane displacement during the first cycle to a displacement ductility of 6. Out-of-plane movement of the T-wall stem was accompanied by an increase in the depth of the compression zone, such that large strains (greater than $8\varepsilon_{cu}$) were measured in the unconfined region of the stem. Out-of-plane displacements returned to approximately

zero when the load was reversed. On the basis of the observed behavior, it was concluded that the code provisions requiring that confinement be provided over half the depth of the predicted compression zone were inadequate and modifications were proposed to the code method for determining the area over which confinement is required. Finally, researchers concluded that the provided volume of transverse hoop reinforcement was adequate and that the presence of flanges limited the potential for catastrophic lateral instability failures seen in planar walls.

## 2.6 Thomsen & Wallace (1995): T-shaped Wall Tests

Planar rectangular and two T-shaped walls were tested at Clarkson University to validate a displacement-based design procedure proposed by the research team. The tests were conducted as part of a larger research effort employing both analytical and experimental investigations. A primary motivation for the research effort was the fact that current codes, such as UBC-91, did not include recommendations for unsymmetrical flanged walls. As a result, a design philosophy employed by engineers with T-shaped and other nonplanar walls was to treat the web and flange(s) as independent rectangular walls that are joined together. The major concerns with this approach were proper detailing and use of a procedure that would adequately predict the effective flange width.

The T-shaped walls were designed to be part of the lateral load resisting system in a six-story prototype building. The walls were nominally identical except for boundary element transverse reinforcement. For the first wall specimen (TW1), the boundary elements in the wall stem (both at the flange-stem intersection and at the stem tip) were design neglecting the influence of the flange on overall wall behavior; this follows the design philosophy in which the wall is treated as two independent rectangular walls. The second wall specimen (TW2) was designed considering the wall as a single component and considering the impact of the flange on the behavior of the stem and vice-versa. Compared to the first wall, the second wall had a significantly larger confined region with greater a volume of transverse reinforcement at the tip of the wall stem and slightly lower volume of transverse reinforcement at the flange-stem intersection.

Experimental results provide improved understanding of T-wall behavior and were used to validate current design philosophies and code design procedures for walls. Under loading putting the flange of the wall in compression, the two walls exhibit similar behavior and very similar flexural strengths. However, under loading putting the tip of the T-wall stem in compression, the impact on performance of the different design philosophies used for the two specimens is evident. The first specimen achieved only 75% of the strength developed by the second specimen. Additionally, the first specimen exhibited a compression-controlled failure followed by rapid strength loss, while the second specimen exhibited a more ductile response with significant lateral strength loss resulting eventually from out-of-plane instability. On the basis of the research results, it was concluded that T-wall boundary element transverse reinforcement may be designed using results of a section analysis for flexure in which a linear strain distribution is assumed (i.e. plane sections are assumed to remain plane) and a conservative estimate of the effective flange width is used. Additionally, test results were used to validate the displacement-based design methodology proposed by the authors; this methodology has since been incorporated in the ACI Building Code.

## 2.7 Brueggen (2009): T-shaped Wall Tests

Two T-shaped walls were tested at the University of Minnesota to investigate the impact of bidirectional lateral loading on the earthquake performance of nonplanar walls. Similar to the Thomsen and Wallace (1995) study, the first T-wall specimen was designed to be part of the lateral load resisting systems for a six-story prototype building and was detailed using the displacement-based design procedure included

introduced in ACI 318-02. The second wall specimen was designed following the first test, with reinforcement design modified to investigate variables of interest. The major parameters that differed between the test specimens were i) the presence of a longitudinal reinforcement splice (Wall 1: no splice, Wall 2: splice at base of second story), ii) distribution of longitudinal reinforcement across the flange in all floors above the second story (Wall 1: concentrated in boundary elements at the flange tips, Wall 2: distributed uniformly across flange), iii) distribution of shear reinforcement in the flange (by volume, Wall 1 has 60% of the reinforcement in Wall 2), and iv) length of the confined boundary element at the tip of the wall stem (for Wall 1 the length is 80% of that used for Wall 2). For each test, the specimen was subjected to a constant axial load of $0.03f_cA_g$ and a prescribed set of displacement cycles at increasing levels of drift demand; the set of displacement cycles included i) one displacement cycle each parallel and perpendicular to the stem of the T-wall, one displacement cycle each at a 45-degree and a 135-degree angle to the stem of the T-wall, and iii) 360 degree bidirectional displacement path that traced the shape of the yield envelope.

The research produced a number of results of interest to the community. First, the research team concluded that because the specimens maintained strength out to the design drift demand, the displacement-based design procedure introduced in ACI 318-02 is appropriate for design of T-walls subjected to bidirectional loading. However, it was noted that T-walls (and other asymmetric nonplanar walls) may not meet the requirements for a tension-controlled section due to a large compression zone depth when the wall flange is in tension; in that case, the ACI 318 displacement-based design procedure is insufficient. Second, shear deformation has a significant impact on strength and stiffness. While all of the longitudinal reinforcement in the effective flange width eventually reaches the yield strain, this does not occur until large drift demands are imposed. At lower drift demands, the steel strain at the flange tips is approximately half the strain at the center of the flange, and the strain distribution is affected by the manner in which longitudinal reinforcement is distributed over the wall cross section. Third, the research team concluded that additional tests of nonplanar walls with different proportions, axial load ratios, and shear-to-moment ratios are necessary to improve understanding of shear-lag effects and wall performance under general loading.

## 2.8 Hosaka et al. (2008): L-shaped Wall Tests

Four L-shape walls were tested by researchers at the University of Tsukuba and Okumura Corporation to investigate methods for improving resistance to compressive-controlled flexural failure and to evaluate the accuracy of fiber-type section analysis. The motivation for this study is the widespread use of core walls in high-rise construction in Japan and the potential for core walls to be subjected to large localized compression demands when loaded at a 45-degrees angle.

Test specimens were 1:6 scale models of the bottom portion of a 30-story prototype building. Each wall specimen was subjected to unidirectional cyclic lateral loading at a 45-degree angle and was subject to axial-to-shear load ratios that ranged from zero when the flange ends were in compression to $0.4\text{-}0.45A_gf_c$ when the wall corner was in compression. Various parameters were examined to evaluate their impact on ductility; these can be grouped into modifications to reinforcement layout and modifications to material strengths. Variations to the reinforcement layout included i) the length of the confined region in the flange ends: Walls 1 and 2 had a confined region that was twice the length of that used for Walls 3 and 4, ii) method of confining the L-shaped corner region: the confined corner region was the same for all walls; however, for Walls 1 and 2, the confined region represented the union of two overlapping rectangular confined regions, while for Walls 3 and 4, the confined region represented the union of three independent square confined regions; iii) vertical spacing of confining reinforcement: spacing was for Wall 2 was 75% of that used for other walls, and iv) addition of high-strength reinforcing

steel in the boundary elements: for Walls 3 and 4 high-strength "axial core" bars were added to each confined region. Major differences in materials properties were i) concrete compressive strength: Wall 3 had a compressive strength 133% of that used for the other specimens, and ii) strength of confining reinforcement: Walls 3 and 4 employed high-strength steel with a yield strength nearly twice that of the reinforcement used in Walls 1 and 2.

All wall specimens exhibited compression failure, characterized by simultaneous crushing of confined concrete and buckling of longitudinal reinforcement in the corner of the wall. However, results support several conclusions about the impact on performance of various parameters. First, Walls 1 and 2 exhibited greater ductility than Walls 3 and 4; this was attributed overlapping rectangular hoops providing better confinement than abutting independent square hoops. Second, the inclusion of high-strength reinforcing bars in the corner of the wall (Walls 3 and 4) increased wall strength when the bars were loaded in tension but had no significant impact on strength when the bars were loaded in compression. Third, for all wall specimens, the vertical strain distribution near the base of all the walls was linear prior to concrete crushing and nonlinear once concrete damage was observed. Fourth, a fiber-type section model in which the strain distribution is assumed to vary linearly over the cross section does not provide accurate prediction of the moment-curvature response near the base of the wall.

## 2.9 Inada et al. (2008) and Kono et al. (2011): L-shaped Wall Tests

Five L-shaped walls were tested at Kyoto University to investigate earthquake behavior and section analysis of L-shaped walls. The research was intended to build on tests of L-shaped walls conducted by Konishi et al. (1997) and Nakachi et al. (1996). The first set of three walls (Inada et al 2008) were 1:4.5 scale and represented L-shaped elements from the bottom three stories of a core-wall lateral system in a 40-story prototype building. The three wall specimens were the same thickness and had the same reinforcement ratios in confined and unconfined regions. All three specimens were subjected to quasi-static unidirectional cyclic loading. Parameters that differed between the three walls were i) length of wall flanges: Walls 1 and 2 had equal length flanges while Wall 3 did not, ii) loading direction: Wall 1 was loaded parallel to one flange while Walls 2 and 3 were subjected to loading at a 45 degree angle, and iii) axial-to-shear load ratio: Wall 1 had an axial-to-shear load ratio that varied from 0.0 when flange ends were in compression to $0.31A_gf_c$ when the wall corner was in compression; for Walls 2 and 3, the ratio varied from 0.0 to $0.26A_gf_c$ . The second set of two L-shaped wall tests (Kono et al 2011) were 1:7.5 scale and represented the bottom six stories of the 40-story prototype structure. The two wall specimens were nominally identical in material properties, dimension, and reinforcement layout; both were subjected to quasi-static unidirectional cyclic loading at a 45-degree angle to the flanges. Wall were subjected to different axial load histories. Both walls were subjected to a linearly varying axial-to-shear ratio, with minimum axial load applied when the tips of the flanges were in compression and maximum axial load applied when the corner of the wall was in compression. For Wall 1, axial load varied from 0.0 to $0.35A_gf_c$; for Wall 2 axial load varied from $0.05A_gf_c$ to $0.50A_gf_c$.

All wall specimens exhibited compression-controlled flexural failure characterized by simultaneous crushing of concrete and buckling of longitudinal reinforcement in the corner of the wall; compression damage was most severe in unconfined regions. Results support several conclusions about behavior and fiber-type analysis of L-shaped walls. First, for specimens subjected to loading at a 45-degree angle putting the tips of the flanges in compression and the corner of the wall in compression, the vertical strain distribution on the cross section remains approximately linear for the entire test; for loading in the opposite direction (tip of flanges in tension and corner in compression), a nonlinear strain distribution is observed at onset of steel yielding or concrete crushing. Second, fiber-type models in

which a linear strain distribution in assumed predict stiffer moment-curvature response than observed near the bottom of the wall in the laboratory. This was attributed to debonding of longitudinal reinforcement and concrete crushing, and revised models that captured these phenomena provided more accurate prediction of response.

## 2.10 Li and Li (2010): L-shaped Wall Tests

Four slender short-limbed L-shaped walls were tested at Xi'an University to investigate the earthquake performance of these components. Per the Professional Standard of P.R. China, short-limbed walls (SLWs) have cross section length-to thickness ratios ranging from 5 to 8 and thicknesses that exceed 200 mm. SLWs are typically utilized as part of the lateral force resisting system in high-rise residential structures as they allow a reduction in the floor area occupied by traditional shear walls with length-to-thickness ratios greater than 8, while providing lateral stiffness that exceeds that of a frame system. Despite significant use in Chinese construction, the seismic performance of L-shaped SLWs is not well understood. The primary objectives of the research were to investigate and characterize nonlinear behavior of L-shaped SLWs including ductility capacity.

The test program investigated the impact on performance of length-to-thickness ratio and axial load ratio. All wall test specimens were 1:2 scale L-shaped walls with equal length flanges. All specimens had uniformly distributed longitudinal reinforcement and confining reinforcement provided over the entire cross section of the wall. Specimens were constructed using concrete and steel with nominally identical properties. All specimens were subjected to quasi-static unidirectional cyclic lateral loading parallel to one flange. To investigate the impact on wall performance of wall length-to-thickness ratio, Walls 1 and 2 were constructed with a length-to-thickness ratio of 5, while Walls 3 and 4 had a ratio of 6.5. To investigate the impact of axial load ratio, walls had different axial loads ranging from $0.1\text{-}0.4f_cA_g$.

The primary observations of the study were as follows: i) all walls exhibited compression-controlled failure characterized by simultaneous crushing and buckling of longitudinal reinforcement in the *tips of the wall flanges*, ii) specimens exhibited an asymmetric load-displacement response, which was attributed to cross sectional configuration, and asymmetry was exacerbated by increased axial load, iii) displacement ductility increased with reduction in the length-to-thickness ratio and the axial load ratio, iv) energy dissipation was increased slightly with increasing wall length-to-thickness ratio. On the basis of the experimental results, the researchers concluded that the earthquake performance of SLWs is superior to that of a traditional shear wall.

## 2.11 Observations and Conclusions about Nonplanar Wall Behavior

The above experimental investigations support a number of significant observations and conclusions about the behavior of nonplanar walls subjected to cyclic lateral loading. These observations and conclusions, which are listed below, have implications for analysis and design. Unfortunately, in many cases, observations suggest that further research is required to fully understand the mechanisms that determine nonplanar wall behavior and advance analysis and design.

- Nonplanar walls respond as a single component with the result that lateral loading that does not activate bending about an axis of symmetry can result in large localized compressive demands. These large compressive demands can result in damage that diminishes strength and deformation capacity or in a compression-controlled failure, which is characterized by rapid strength loss and low drift capacity.
- The potential for compression-controlled failure is exacerbated by increased axial load.

- Multiple experimental studies have investigated design criteria for confining reinforcement in walls. Early tests validated current ACI Code requirements. However, more recent tests have shown the potential for compression-controlled failure of well-confined walls. Typically, this has been due to either increased axial load demand or adverse lateral load orientations.
- For symmetric wall configurations in which flanges carry compression and do not exacerbate local compressive demands (e.g., I- and H-shaped walls), flanges can improve out-of-plane stability, especially in comparison with planar or asymmetric walls with narrow compression regions.
- Multiple nonplanar walls have exhibited web crushing failures in the vicinity of the flange-web interface. This has been attributed to high compression demands resulting from shear transfer within a small compression-region of the wall web.
- Since shear transfer occurs via compression struts, shear transfer in flanged walls can result in shear transfer occurring over a small compression region within the wall cross section. This has significant implications for shear design and assessment of shear capacity.
- Shear transfer in flanged walls can result in undesirable deformation modes including out-of-plane bending of flanges and sliding at the web-foundation interface.
- Multiple tests of nonplanar walls of varying configurations show that shear can result in nonlinear vertical strain distributions across wall cross-sections; companion studies have shown that for these systems, response prediction based on the assumptions that shear deformations are negligible and plane section remain plane is inaccurate.
- Ile and Reynouard (2005) and Lowes et al. (2014) each provide data characterizing the response of three nominally identical C-shaped walls subjected to different unidirectional and bidirectional lateral load histories. Data from both tests show that in comparison with specimens subjected to unidirectional loading, bidirectional loading results in reduced drift capacity.

# 3 BEHAVIOR OF U-SHAPED AND C-SHAPED WALLS

The above review of previous experimental research provides general understanding of nonplanar wall behavior. To provide additional context to the C-shaped wall tests presented in Lowes et al. (2014), a detailed presentation of the behavior of the U-shaped wall tests conducted by Beyer et al. (2008) and Ile and Reyounard (2005) is presented below. Section 3.3 summarizes observations of the three C- and U-shaped wall test programs.

## 3.1 Beyer et al. (2008): U-shaped Wall Tests

Beyer et al. tested two U-shaped walls (TUA and TUB) to provide understanding of the impact of design and load parameters on performance. The two walls were identical with the exception that Specimen TUB was thinner than Specimen TUA. Both specimens were subjected to bidirectional lateral loading and constant axial load. Lateral loading was applied under displacement control and followed the displacement pattern shown in Figure 1. The same axial load was applied to both specimens; this represented an axial load of $0.02f_cA_g$ for TUA and $0.04f_cA_g$ for TUB. Differences in wall thickness resulted in the two specimens exhibiting different failure mechanisms. Specimen TUA failed due to fracturing of longitudinal bars in the boundary elements at the tips of the flange, while Specimen TUB failed due to crushing of unconfined concrete in the web outside the boundary elements. The behavior of these two walls is described below.

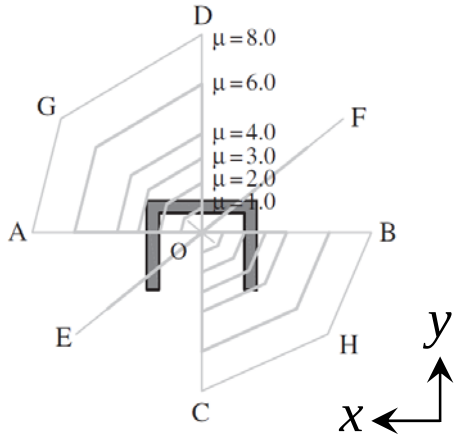


**Figure 1: Loading protocol for Specimens TUA and TUB tested by Beyer et al. (2008). Note that for each ductility demand, testing progressed as O-A-B-O, O-C-D-O, O-E-F-O, O-A-G-D-C-H-B-O.**

### 3.1.1 Specimen TUA

Figure 2 shows, for Specimen TUA, normalized response histories for four phases of the laboratory load history. Load is presented as the applied base moment normalized by the maximum flexural strength of the section as computed using Response2000 (http://www.ecf.utoronto.ca/~bentz/r2k.htm) and considering the impact of shear. Markers on the plots indicate when yielding, failure and intermediate damage states occurred.

For Specimen TUA, damage progressed as follows. Initial (theoretical) yield occurred at 0.25% drift. Spalling initiated during cycles to 1% drift (All plots: DS1) and became widespread during cycles to 1.25% drift (All plots: DS2). During cycles to 1.8% drift for strong-axis bending and 2% drift for positive and negative weak axis bending, sliding along the interface, buckling of the longitudinal bars in the flange toe BE's, and minor spalling in the unconfined regions of the web adjacent to the corner BE's ere observed (All plots: DS3). During cycles to 2.5% drift in strong axis bending, longitudinal bars in the West flange fractured (Strong-Axis: Failure). The positive-weak axis failed due to the fracture of previously buckled bars in the flange toe BE's (Weak-Axis: Failure). A significant loss in load-carrying capacity was observed under subsequent loading in the diagonal direction. The last cycle in the negative diagonal direction caused fracture of previously buckled web bars (Strong-Diagonal, Weak-Diagonal: DS4). After load reversal to the positive diagonal, all remaining bars in the West flange web fractured as well as three additional longitudinal bars in the West flange toe BE (Strong-Diagonal, Weak-Diagonal: Failure).

Boundary elements at the toes of the flanges exhibited extensive spalling and rupture of the end boundary element bars. However, concrete within the toe boundary elements remained well confined and no concrete crushing was observed. Sliding was observed at large displacements, even with shear keys used in the design of the specimens. One of the shear keys was observed to have sheared off; other shear keys were not visible. Some compressive damage was visible along the web between the corner boundary elements and on the east flange web, although the researchers did not observe an impact on the failure mechanism from this damage.

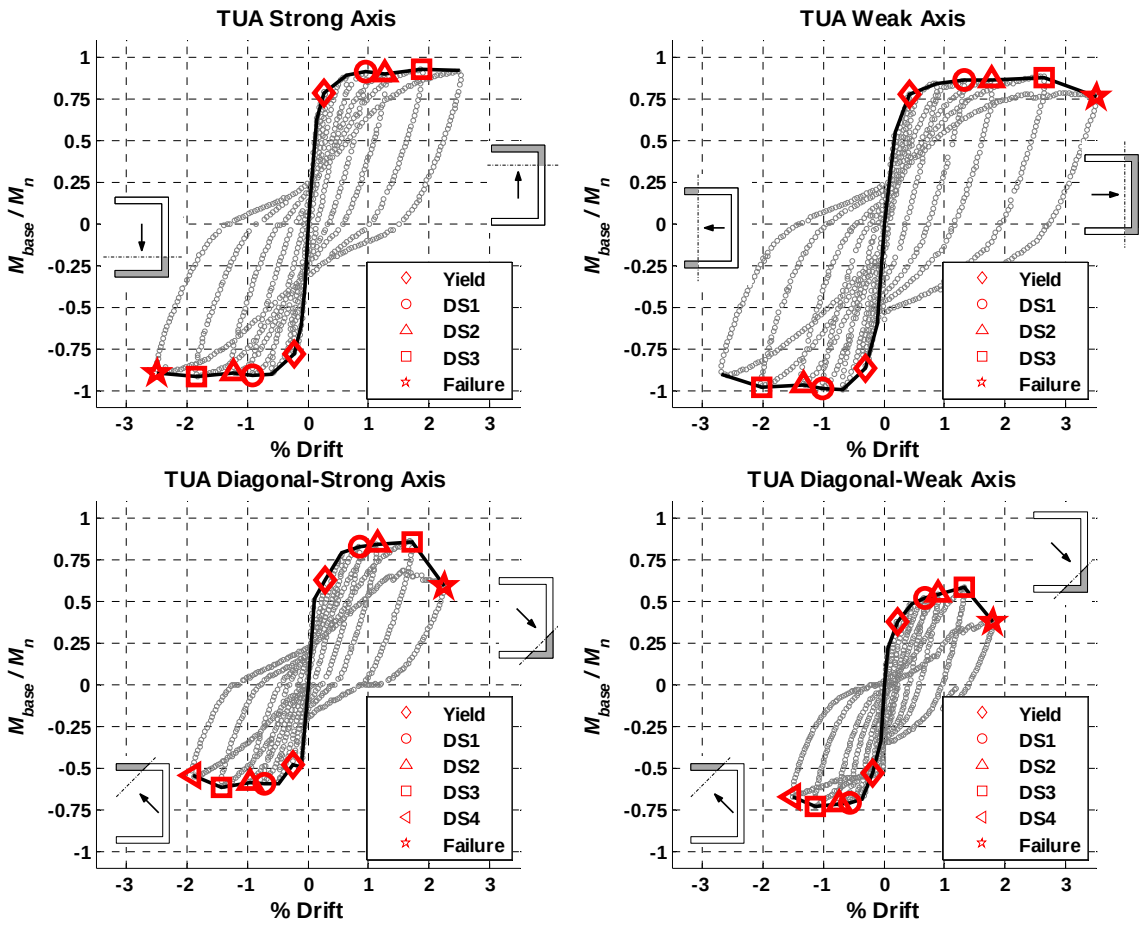


Figure 2: Specimen TUA load-deformation response (Beyer et al. 2008). Note that Yield indicates theoretical first yield of longitudinal steel, DS1 indicates initial spalling, DS2 indicates significant spalling, DS3 indicates buckling of longitudinal steel, DS4 indicates fracture of longitudinal steel, and Failure indicates significant loss in lateral load carrying capacity.

### 3.1.2 Specimen TUA: strength and ductility

The load-deformation response for loading parallel to the web of the wall (activating strong-axis bending) shows a well-defined yield plateau with minimal cyclic strength degradation. Some pinching of the hysteretic response is observed, becoming pronounced as early as 1% drift. The specimen reached a maximum strength equal to approximately 83% of computed nominal strength; results do not suggest an obvious reason for reduced capacity. For loading parallel to the web of the wall, the specimen achieved a drift capacity of 2.5%.

The load-deformation response for loading perpendicular to the web of the wall (activating weak-axis bending) has a defined yield plateau with some strength loss due to cyclic loading. The specimen reaches approximately 86% of the nominal moment capacity for loading putting the web in compression and 100% of nominal moment capacity for loading putting the tips of the flanges in compression; results do not suggest an obvious explanation for the difference in strength in the two loading directions. Unloading in the positive direction resulted in significant residual deformations at zero force after cycles to 1% drift. The specimen achieved a drift capacity of 3.5% for loading putting the web in compression and 2.8% for loading putting the tips of the flanges in compression.

For loading at 45 degrees to the principal axes, reduced ductility, strength and energy dissipation is observed. For loading along both diagonal paths, data show drift capacities of less than 2% and a strength loss of 20-25% in comparison with strength under uni-directional loading. The positive diagonal (East flange corner in compression) performs marginally better than the negative diagonal (West flange toe in compression), which can be attributed to the smaller compressive region in the toe BE and consequential damage occurring.

### 3.1.3 Specimen TUB

Specimen TUB was subjected to the same lateral displacement history as Specimen TUA and a constant axial load of $0.04f_cA_g$. Normalized load versus drift plots for four phases of loading are shown in Figure 3. Loads were normalized and drifts computed using the same process as used for Specimen TUA

For Specimen TUB, damage progressed as follows. After reaching initial (theoretical) yield at approximately 0.4% drift, spalling initiated during cycles to 1.25% drift (All plots: DS1). Spalling exposing longitudinal reinforcement during cycles was observed during cycling to 1.65% drift (All plots: DS2). Spalling spread into the unconfined web regions during subsequent cycles resulting in a significant loss of sectional width in some unconfined areas. The web's ability to carry compression across the damaged unconfined regions failed during the cycles at 2.5% drift in the strong-axis direction. Web-crushing resulted in a new load path within the specimen for the lateral shear. Specifically, a frame mechanism developed in which shear was transferred to the foundation via bending of the corner boundary elements and transverse shear loading of the compression flange. This frame mechanism is shown in Figure 4(b). Bar buckling was observed in the West flange toe BE during the final cycles. No loss of confinement or crushing in the BE's was observed. No reinforcing bars fractured and the maximum sliding displacement was 4.4% of the total drift.

### 3.1.4 Specimen TUB: strength and ductility

Specimen TUB presented a similar load-deformation response to TUA. For loading parallel to the web of the wall activating strong-axis bending, the response history has a well-defined yield plateau and no strength degradation under cyclic loading. A strength equal to 86% of the nominal capacity is reached; again there is no obvious explanation for the reduced strength. A drift capacity of 2.5% is observed.

For loading perpendicular to the web of the wall, activating weak-axis bending, again the response history has a well-defined yield plateau with some strength loss due to cyclic loading. For loading putting the web in compression, a strength equal to 91% of nominal strength is achieved; while for loading putting the tips of the flanges in compression a strength equal to 100% of nominal strength is achieved. This is similar to the response of TUA; as with specimen TUA, results do not suggest an obvious explanation for the difference in strength in the two loading directions. Unloading from the positive direction resulted in significant residual deformations at zero force after cycles to 1.5% drift. Drift capacities for weak axis bending are similar to those observed for TUA; a drift capacity of 3.0% (3.5% for TUA) is observed for loading putting the web in compression, and a drift capacity of 2.8% (2.8% for TUA) is observed for loading putting the tips of the flanges in compression.

The response of specimen TUB to loading at a 45 degree angle to the principal axes was similar to that of specimen TUA. Though, where specimen TUA showed some strength loss in the penultimate load cycle, specimen TUB showed no strength loss.

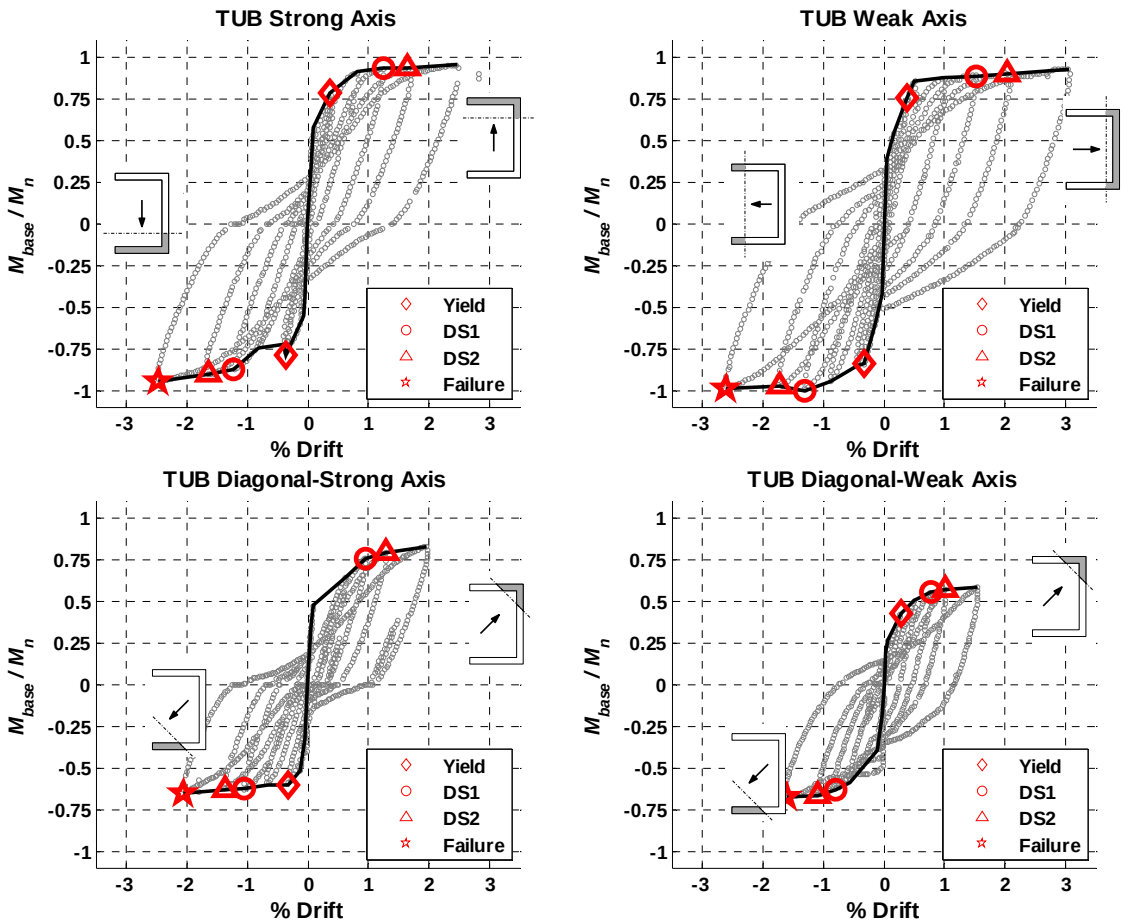


**Figure 3: Specimen TUB load-deformation response (Beyer et al. (2008). Note that Yield indicates theoretical first yield of longitudinal steel, DS1 indicates initial spalling, DS2 indicates significant spalling exposing longitudinal steel, DS3 indicates buckling of longitudinal steel, DS4 indicates fracture of longitudinal steel, and Failure indicates significant loss in lateral load carrying capacity.**

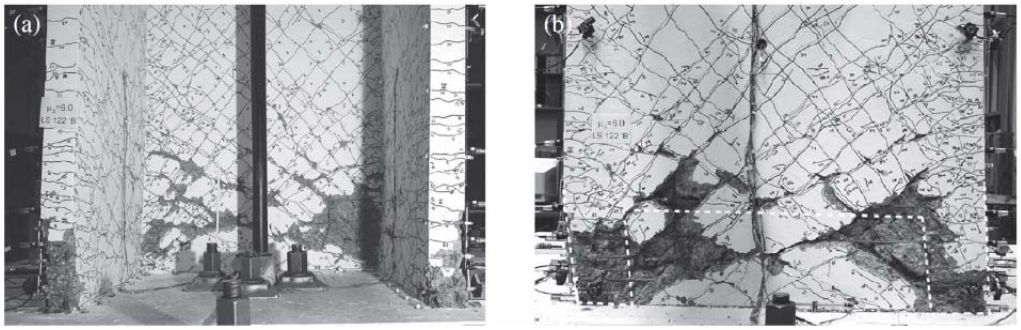


**Figure 4: TUB south face (a) and north face (b) during loading to μ = 6. The dashed line illustrates the frame mechanism (from Beyer et al. 2008).**

### 3.1.5 Beyer et al. (2008): Observations and conclusions about wall behavior

Experimental tests conducted by Beyer et al. support several significant observations about nonplanar wall behavior and the impact of bidirectional loading:

1. Well-detailed modern walls can maintain strength to moderate ductility and drift demands (TUA maintained strength to a displacement ductility of 4 and drift demands parallel and perpendicular to the wall web of ~2.5%).
2. There is the potential for general bidirectional load histories to produce large localized compressive demands that, in turn, produce compression damage or failure.
3. Shear load paths and shear response mechanisms can be complex in nonplanar walls subjected to general bidirectional loading.

## 3.2 Ile and Reyounard (2005): U-shaped Wall Tests

Ile and Reyounard (2005) present the results three U-shaped wall tests conducted at the European Laboratory for Structural Assessment (ELSA). The walls were nominally identical, but were subjected to different lateral load patterns. IleX was subjected to lateral loading parallel to the web of the wall activating strong-axis bending; IleY was subjected to lateral loading parallel to the flanges of the wall activating weak-axis bending. IleXY was subjected to the lateral load pattern shown in Figure 5. All tests employed quasi-static cyclic lateral loading combined with constant axial load; the axial load ratio for the specimens ranged from 0.1 to 0.12. Figure 6 shows response histories for each of the test specimens; to facilitate comparison, response histories for strong- and weak-axis bending of IleXY are presented.

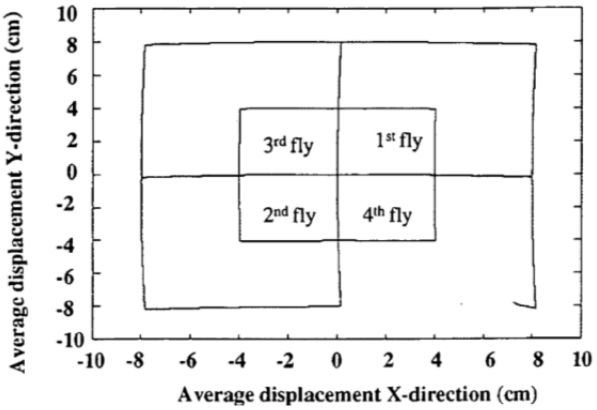


**Figure 5: Lateral displacement pattern for U-shaped wall tests presented by Ile and Reynouard (2005).**

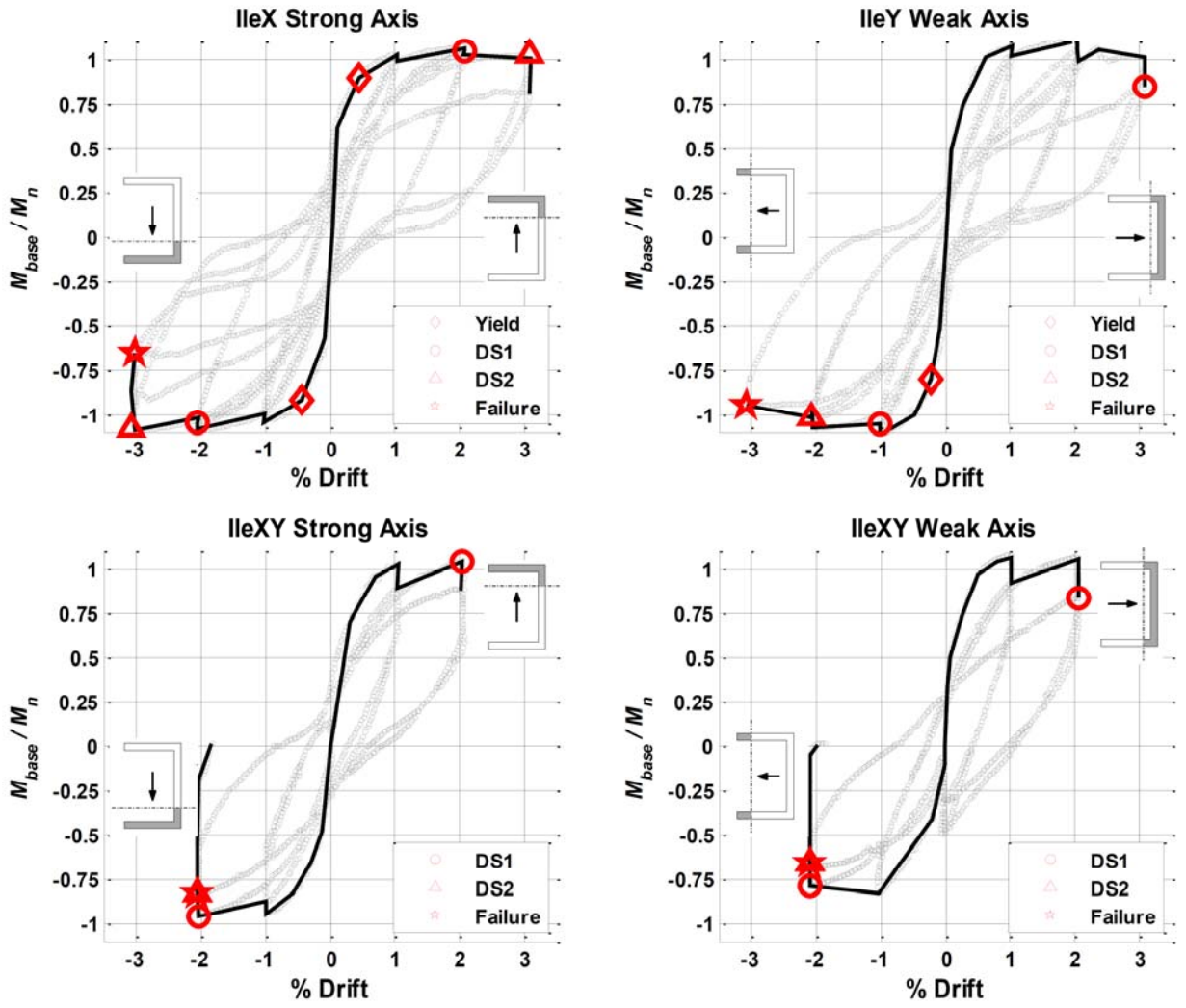


**Figure 6: Normalized base moment versus drift for U-shaped wall tests presented by Ile and Reynouard (2005). Note that Yield indicates theoretical first yield of longitudinal steel, DS1 indicates onset of bar buckling, DS2 indicates rupture of transverse reinforcement, and Failure indicates significant loss in lateral load carrying capacity.**

### 3.2.1 Specimen IleX

Specimen IleX was loaded uni-directionally parallel to the web of wall activating strong-axis bending. Theoretical yield of reinforcing steel occurred at 0.43% drift. Damage beyond cracking was reported to initiate during cycles to 2% drift with bar buckling occurring in the BE at the ends of the flanges (IleX: DS 1). After two cycles to 3% drift, damage was characterized by severe bar buckling, rupture of BE stirrups and rupture of BE longitudinal bars at the ends of both flanges and the corners (IleX: DS2). In the final cycle to 3% drift, failure resulted from rupture of previously buckled longitudinal bars in the flange (IleX: Failure).

### 3.2.2 Specimen IleY

Specimen IleY was loaded uni-directionally parallel to the flanges of the wall activating weak axis bending. Theoretical yield of reinforcing steel was reached at 0.23% drift in the negative direction (toe in compression). Damage was reported to initiate at 1% drift with bar buckling at the ends of both flange

BE's, similar to specimen IIeX (IIeY: DS 1). The wall continued to perform well for one full cycle at 3% drift. A compression-controlled failure occurred during the second cycle to negative 3% drift. Simultaneous buckling of reinforcing bars and concrete crushing was observed in the BE at the tip of one flange (where the stirrup at the base of the wall was missing due to a construction error); following failure of one BE, reinforcement in the other flange BE buckled and the stirrup fractured (IIeY: Failure). Upon unloading and reloading in the positive direction, flange-tip reinforcement fractured.

### 3.2.3 Specimen IIeXY

Specimen IIeXY was loaded bi-directionally in a butterfly pattern (Figure 5). Damage was reported to be widespread by the first cycle to 2% drift with extensive spalling, bar buckling and fracture occurring (IIeXY: DS1). The specimen failed in the last cycle while at 2% drift in the strong axis and 2% drift in the negative weak axis (East flange toe in compression) with the fracture of three previously buckled BE bars on the West flange followed by a shear failure of the flange (IIeXY: Failure).

### 3.2.4 Ile and Reynouard (2005): Observations and conclusions about wall behavior

Experimental tests presented by Ile and Reyounard support the primary observations of the Beyer et al. study. Specifically, similar to Beyer et al. (2008), the data show

1. Well-detailed modern walls can maintain strength to moderate ductility and drift demands. Here the specimens maintained strength to a displacement ductility of approximately 6 and a drift capacity of 3%.
2. There is the potential for general bidirectional load histories to produce large localized compressive demands that, in turn, produce compression damage or failure. Here weak-axis bending of IIeY induced severe compression demand on the toes of the BE flanges (though a construction error likely caused premature failure)
3. Shear transfer mechanisms are complex in nonplanar wall subjected to bidirectional loading.

Additionally, given the complexity of shear transfer mechanisms and the potential for shear transfer to occur over relatively small compression zones, Ile and Reyounard recommend that more conservative approaches to assessing shear capacity be employed for design.

## 3.3 Comparison of Bidirectionally Loaded C- and U-shaped Walls

To further investigate the impact of bidirectional loading on wall response, normalized moment versus drift data for the C- and U-shaped wall tests by Lowes et al. (2014), Beyer et al. (2008) and Ile and Reynouard (2005) were compared. Figure 7 shows the envelopes to the cyclic normalized moment versus drift data for all C- and U-shaped walls for loading parallel to the web of the wall activating strong-axis bending; Figure 8 shows similar data for loading perpendicular to the web of the wall activating weak-axis bending.

For strong-axis bending (Figure 7), despite significant differences in geometry, material properties, design and load histories, normalized load versus drift response is similar up to 0.75% drift. In this range, all walls reaching 80-90% of nominal flexural strength and exhibit a well-defined yield plateau. Drift capacity, however, varies significantly (1% to 3%) for the different specimens and test programs. Within individual test programs, comparison of unidirectionally and bidirectionally loaded specimens (CW6 vs CW7 and CW8; IIeX vs IIeXY) shows bidirectional loaded walls have reduced drift capacity.

For weak axis bending (Figure 8**Error! Reference source not found.**), there is more variability in the normalized response envelopes. All specimens again reach 80-100% of nominal strength and most specimens exhibit a well-defined yield plateau. However, there is significant variation in stiffness, and

moderate variation in drift capacity (2% - 3%). Further research is required to determine the factors that determine stiffness and drift capacity.

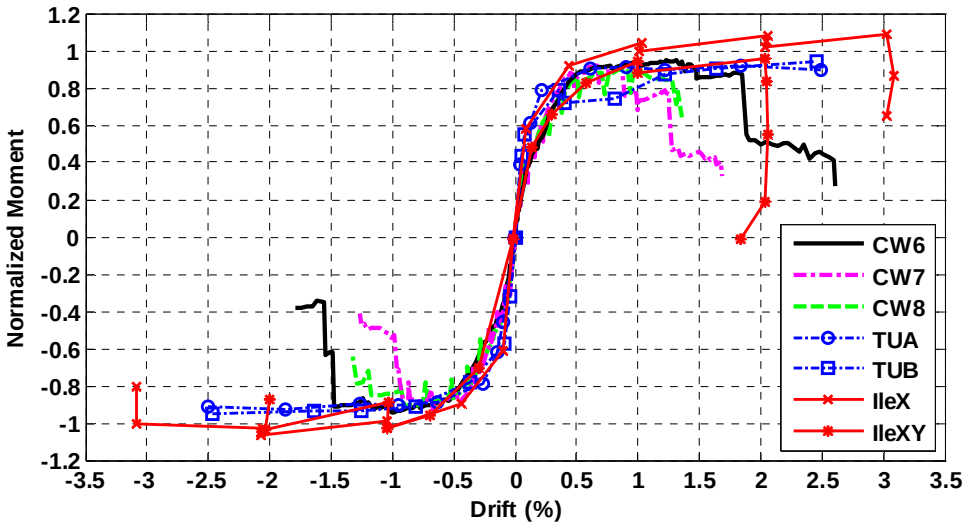


**Figure 7: Comparison of strong-axis load-drift response**

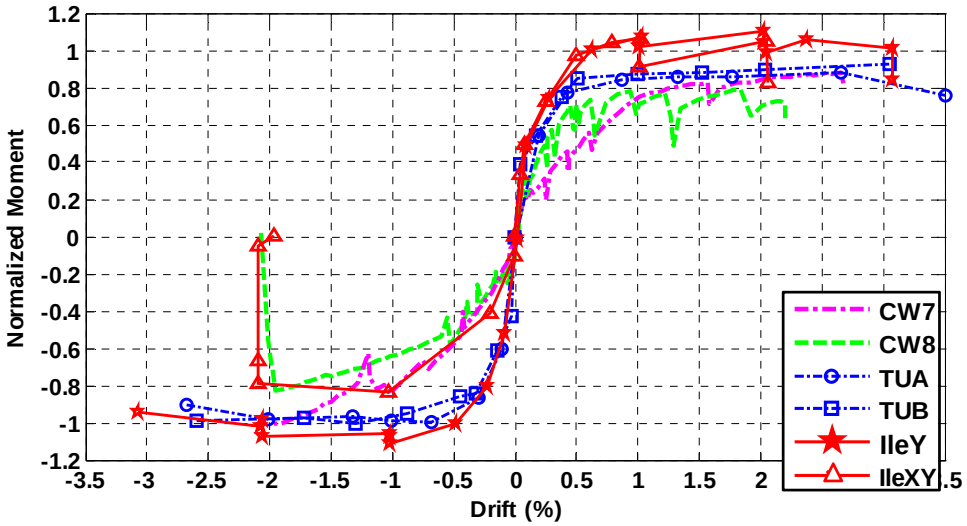


**Figure 8: Comparison of weak-axis load-drift response**

## 4 FAILURE MECHANISMS FOR NONPLANAR WALLS

To support assessment of the impact of design parameters on performance, the failure mechanism of each nonplanar was determined by examining the photos and damage narratives provided by the researchers. A specimen was considered to fail if, under loading to new maximum displacement demand, strength was less than 80% of the historic maximum measured strength. A failure mechanism was denoted for each direction of loading for which the 20% strength loss criterion was met. Three primary failure mechanisms were identified; these were classified as “buckling-rupture”, “crushing-buckling”, and “shear-compression” failures. In addition, three secondary failure mechanisms, which were observed to contribute significantly to the primary failure mechanisms, were classified as “framing action”, “sliding”, and “failure of confinement”. The primary and secondary failure mechanism exhibited by the test specimens are listed in Table 3 below; detailed discussions of the various mechanisms follow.

**Table 3: Primary and Secondary Failure Mechanism Exhibited by Nonplanar Wall Specimens**

| Researcher | Specimen | Primary Mechanism | Secondary Mechanisms | Description |
|---|---|---|---|---|
| **Beyer et al.** | **TUA** | BR | Sliding | |
| | **TUB** | SC | Frame mech. | |
| **Ile and Reynouard** | **IleX** | BR | | Three longitudinal bars in the flange buckled and subsequently ruptured on the following cycle during straightening. |
| | **IleY** | BR | | One flange tip lost confinement due to stirrup rupture and BE vertical bars ruptured after buckling. |
| | **IleXY** | BR | | Three longitudinal bars in the flange buckled and subsequently ruptured on the following cycle during straightening. |
| **Lowes et al.** | **CW6** | BR | Sliding, frame mech., stirrup slip | |
| | **CW7** | BR | Sliding, frame mech., stirrup slip | |
| | **CW8** | BR | Sliding, frame mech., stirrup slip | |
| **Brueggen** | **NTW1** | CB | Stirrup slip | |
| | **NTW2** | CB | Stirrup slip | |
| **Oesterle et al.** | **F1** | SC | Sliding, frame mech. | |
| | **F2** | SC | Sliding, frame mech. | |
| **Thomsen and Wallace** | **TW1** | CB | | Brittle buckling failure characterized by sudden concrete cover loss, and buckling of vertical bars predominantly in BE and fewer in web. |
| | **TW2** | CB | | Specimen experienced global buckling failure due to out-of-plane instability in the web boundary element. |
| **Inada** | **L00A** | CB | | Crushing followed by shear failure near wall base. |
| | **L45A** | CB | | Crushing in both corner BE and unconfined web led to failure. On load reversal shear sliding failure occurred near wall base. |
| **Kono** | **L45C** | CB | | Concrete crushing in corner BE accompanied by crushing of compression strut. |
| | **L45D** | CB | | |
| **Funaki** | **L1** | CB | | Compression failures occurred in corner BE of wall, and for L1 and L2; crushing progressed into unconfined web region. |
| | **L2** | CB | | |
| | **L5** | CB | | |
| | **L6** | CB | | |
| **Li** | **DL1** | BR | | |
| | **DL2** | BR | Stirrup slip | |
| | **DL3** | CB | | |
| | **DL4** | CB | | |

## 4.1 Primary Failure Mechanisms for Nonplanar Walls

### 4.1.1 Buckling-rupture (BR)

The buckling-rupture failure is characterized by the rupture of BE vertical reinforcing bars that previous buckled under compressive loading. This failure mechanism is initiated by spalling and outward buckling of vertical reinforcing bars under flexural compression loading. Upon load reversal, bars straighten under tension loading, local plastic strain demands in the bar are excessive and the bar ruptures. The BR failure may or may not be accompanied by crushing of confined BE concrete. The detailing of boundary element stirrups and the buckling length of the vertical bars were observed to be important factors in the onset of this failure mechanism. This failure mechanisms was observed primarily in C-shaped and U-shaped wall configurations. An example of the buckling of vertical BE reinforcing bars followed by rupture during straightening in shown in Figure 9.

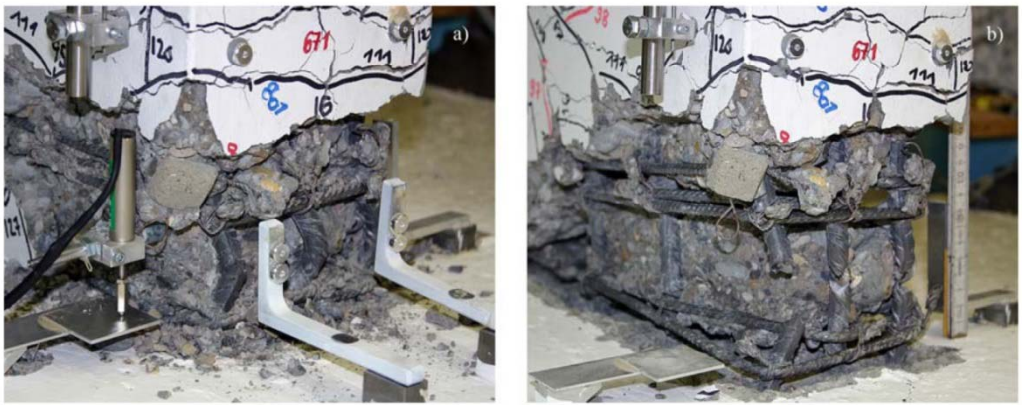


**Figure 9: Example of buckling-rupture failure from Beyer et al. (2008) – Specimen TUA**

### 4.1.2 Crushing-buckling (CB)

The crushing-buckling failure is characterized by crushing of the concrete in the BE core and buckling of the vertical BE reinforcing bars. The mechanism initiates with spalling of BE cover concrete. The spalling is often severe and extends a significant distance up the height of the wall and into the unconfined web of the wall. The BE then exhibits a loss of confinement due to failure confining stirrup(s). Subsequently, some wall specimens with CB failures exhibited a sudden loss of load capacity by out-of-plane buckling of the entire boundary element, while other specimens progressively lost capacity as the core concrete crushed. This failure mechanisms was observed primarily in T-shaped and L-shaped wall configurations. Two examples of a CB failure are shown in Figure 10.

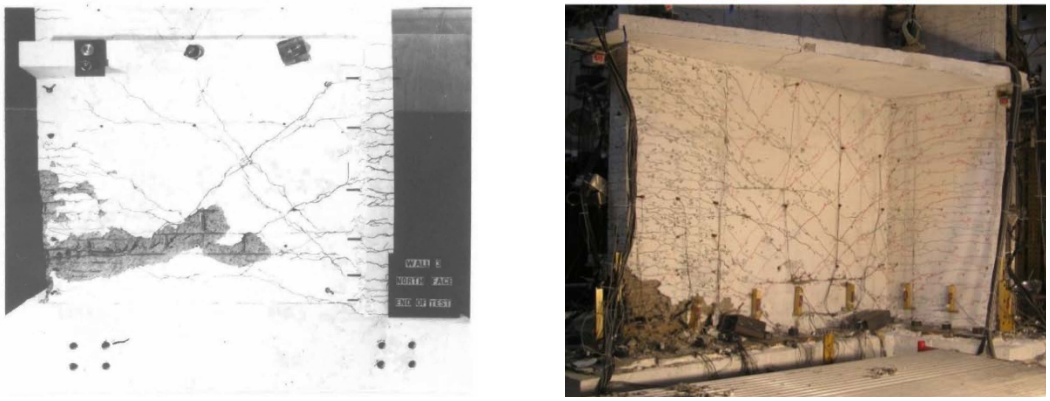

(a) Paulay and Goodsir (1985) (b) Breggen (2009) - Specimen NTW2

**Figure 10: Examples of crushing-buckling failures**

### 4.1.3 Shear-compression (SC)

The shear compression failure is characterized by crushing of the concrete between the boundary element zones of a wall. For walls with significant shear demand, a diagonal compression strut flowing across the web into the boundary element results in spalling and significant crushing of the panel zone concrete. The panel zone damage results in loss of stiffness and load carrying capacity. The panel zone between boundary elements has no confinement of the concrete and larger spacing between the horizontal and vertical bars. The large spacing in the panel zone was observed to cause more severe spalling where the crack may form deeper than clear cover. In addition, the cyclic loading of walls causes sliding along the diagonal cracks of the wall that further degrades the web's ability to transfer compression. This failure mechanism was observed primarily in H-shaped, C-shaped and U-shaped wall configurations. Two examples of a shear-compression failure are shown in Figure 11.

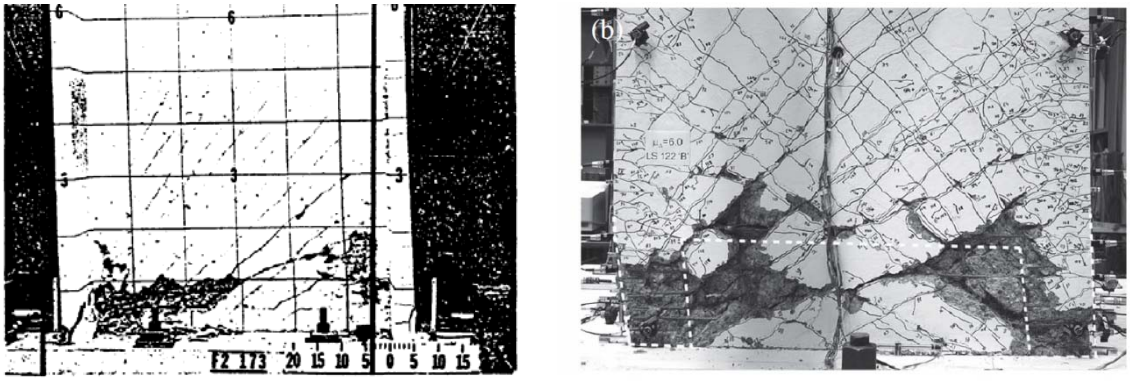


(a) Oesterle (1979) - Specimen F2 (b) Beyer et al. (2008) - Specimen TUB

**Figure 11: Examples of shear-compression failures**

## 4.2 Secondary Failure Mechanisms

Following onset of the primary failure mechanisms, secondary failure mechanisms develop and contribute to strength and stiffness loss under continued loading.

### 4.2.1 Framing action

Framing action refers to stiffness and strength loss associated with damage to the unconfined web region of the wall that results in shear load being transferred via "frame-action" of the boundary elements at the perimeter of the wall. Figure 11(b) shows an example of this mechanism. Damage due to spalling in the unconfined web region of a wall causes reduces stiffness and reduced compression-strut capacity. Stiffness and strength loss can be severe as the larger spacing of horizontal and vertical reinforcing bars in the unconfined web can result in concrete spalls that penetrate deep into the wall cross section. As damage increases, at the base of the wall, the boundary elements begin to act as independent columns that are connected by the upper, undamaged portion of the wall. The increased flexure and shear demand on the boundary elements, as load is transferred from the web of the wall to the boundary elements, contributes BE damage and failure. Typically framing action is observed in shear-compression failures, however it was also observed in walls with buckling-rupture failures. Framing action was observed in specimens with significant sliding as well as negligible sliding and, thus, both are included as secondary mechanisms.

### 4.2.2 Sliding

Sliding may occur at the wall- foundation interface. Typically, the wall-foundation interface is a cold-joint in the concrete. This and the geometry and loading of the system typically result in the wall-foundation interface being the site of a wide crack. Separate concrete pours for the wall and foundation reduce aggregate interlock across this interface, and shear resistance at the interface typically is provided by friction and dowel action of the vertical reinforcing bars. Often sliding initiates in the unconfined web of the wall where longitudinal reinforcement is lighter; sliding in the region increases shear demand in the BEs and transverse flanges, if present. Dowel action of BE reinforcement results in increased deformation demands for BE bars, and the potential increased local plastic strain demand and premature bar fracture. Under cyclic loading, dowel action in longitudinal reinforcement can degrade the surrounding concrete, further deteriorating stiffness and strength. Sliding may be associated with all of the primary failure mechanisms. An example of sliding is shown in Figure 12.

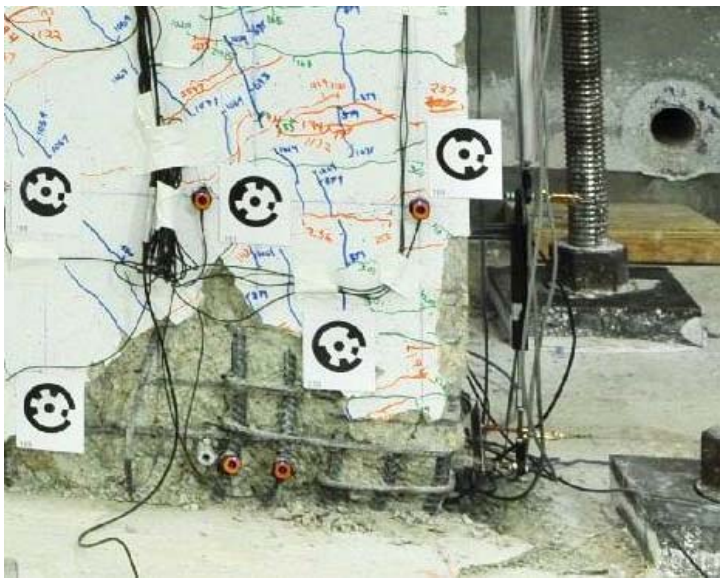

(a) Dowel action of the BE bars

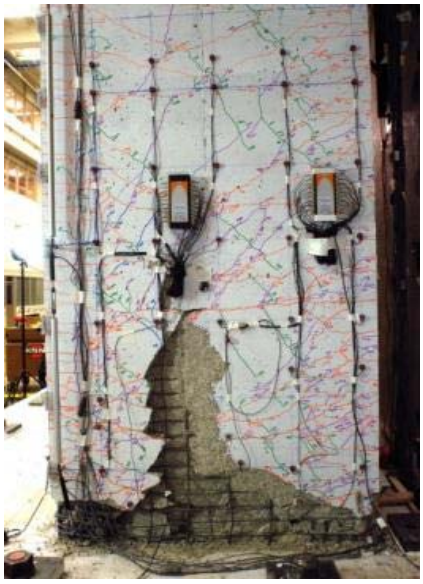

(b) Transverse shear in flange

**Figure 12: Examples of damage due to sliding**

### 4.2.3 Failure of confinement

Modern design codes required that confining reinforcement terminate with 135-degree hooks with hook ends embedded in core concrete. This is intended to ensure that confinement is not lost prematurely due to unwrapping of a hoops or anchorage failure of confining hooks. However, laboratory tests show that crushing of core concrete can be sufficiently severe that confinement does not fracture but instead exhibits anchorage failure. Figure 13 below shows examples of this type of failure (Brueggen 2009). Typically, this mechanism is associated with the BR and CB failure modes.

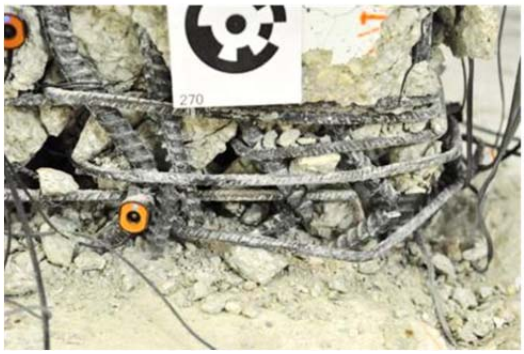

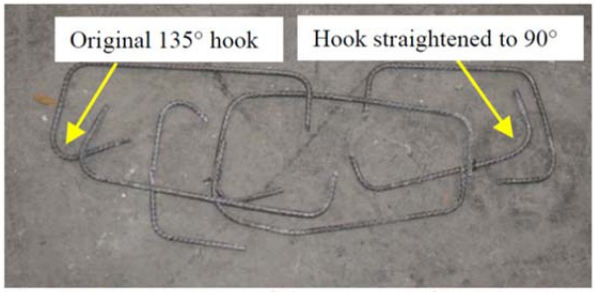


Figure 5.25. Damage to confining hoops near foundation block.

**Figure 13: Examples of confinement failure (Brueggen 2009)**

## 5 INVESTIGATION OF NONPLANAR WALL DESIGN AND RESPONSE PARAMETERS

Here, correlations between various simple design parameters and wall ductility and failure mechanism are investigated. Results are compared with those from a similar study of planar walls. Given that experimental data show complex strain profiles, damage patterns and failure mechanisms in nonplanar walls subjected to cyclic bidirectional loading, the expectation is that correlation between simple design parameters and observed response will be weak. However, the value to the engineering community of identifying these correlations is high.

## 5.1 Description of Wall Design and Response Parameters.

Eighteen parameters were used to characterize the nonplanar wall specimens. Table 4 defines design parameters characterizing wall geometry, wall reinforcement and loading conditions. Table 5 defines parameters determined from moment-curvature analyses of the wall cross sections, and Table 6 lists computed quantities for all specimens. Moment-curvature analysis was accomplished using the Response2000 software, which employs a fiber-type section model and includes non-linear concrete and steel constitutive models. The concrete model included the effects of compression softening and tension stiffening, but not the impact of confinement on concrete compression response. A tri-linear reinforcing steel model was used to simulate yielding and strain hardening. With the goal of simplifying the analyses, the impact of cyclic loading, bi-directional loading and shear-flexure interaction were not considered in the analyses. For these analyses, nominal moment strength was defined as the strength when the strain in the extreme concrete compression fiber was -0.003; this is consistent with ACI 318.

**Table 4: Design parameters characterizing wall configuration and loading**

| Parameter | Symbol | Definition |
|---|---|---|
| Scale | Scale | Specimen scale defined as the thickness of the wall parallel to the direction of loading divided by the thickness of a full scale wall, considered to be 12 in. |
| Shear span ratio | $M/(Vl_w)$ | The ratio of effective height of loading (M/V) to the length of the wall parallel to the direction of loading. For bi-directionally loaded walls, this value was defined separately for each direction of loading. |
| Axial load ratio | $\lambda_N$ | The applied axial load (N) divided by the gross axial capacity (Agf'c). For walls with varying axial load, this parameter was defined by the load applied at zero drift. |
| Concrete strength | $f_c'$. | The experimentally measured compressive strength. |
| Vertical reinforcement ratio | $\rho_v$ | The total area of vertical reinforcing steel divided by the gross sectional area. |
| BE vertical reinforcement ratio | $\rho_{be}$ | The area of vertical reinforcing steel in the boundary element divided by the boundary element area. For walls with multiple boundary elements the average value was used. |
| BE volumetric reinforcement ratio | $\rho_{con}$ | The volume of horizontal confining steel contained the boundary element divided by the volume of concrete enclosed by the boundary element. For walls with multiple boundary elements, the average value was used. |
| Horizontal reinforcement ratio | $\rho_h$ | The area of horizontal reinforcing steel divided by the area of concrete in the web wall parallel to the direction of loading. For bi-directionally loaded tests, this values was defined separately for each direction of loading. |
| Nominal shear stress | $V_n/\left(A_{cv}\sqrt{f_c'}\right)$ | The nominal shear stress where the nominal shear strength, Vn, and shear area, Acv, are defined by ACI 318. For bi-directionally loaded tests, the value of Vn and Acv was defined separately for each direction of loading. |
| Normalized shear strength | $V_u/V_n$ | The maximum measured shear, Vu, divided by the nominal shear strength per ACI 318, Vn. |

**Table 5: Design parameters characterizing flexural response**

| Parameter | Symbol | Definition |
|---|---|---|
| Normalized moment strength | $M_u/M_n$ | The maximum measured moment capacity, Mu, divided by the nominal moment strength. |
| Compressive strain at yield | $\varepsilon_c$ | Strain in extreme concrete compression fiber at first yield of extreme tensile reinforcement. |
| Depth of compression at yield | $c_{yield}/l_w$ | The depth of compression zone at first yield of the extreme tensile reinforcement divided by the length of the wall parallel to the direction of loading. |
| Curvature at yield | $\phi_y$ | The curvature at the yield of the extreme tensile reinforcement. |
| Tensile strain at nominal | $\varepsilon_t$ | Strain in the extreme tensile reinforcement at nominal moment strength. |
| Normalized tensile strain at nominal | $\varepsilon_t/\varepsilon_y$ | The tensile strain at nominal moment strength divided by the yield strain of the reinforcing bars. |
| Depth of compression at nominal | $c/l_w$ | The depth of compression zone at the nominal moment strength divided by the length of the wall parallel to the direction of loading. |
| Curvature at nominal | $\phi_n$ | The curvature at nominal moment strength. |

**Table 6: Results of Moment-Curvature Analysis**

| Researcher | Name | $M_u/M_n$ | $V_u/V_n$ | $\varepsilon_t$ ($\mu$s) | $\varepsilon_t/\varepsilon_y$ | $c / l_{web}$ | $\phi_{Nom}$ (rad) | $\varepsilon_c$ ($\mu$s) | $c_{yield} / l_{web}$ | $\phi_{Yield}$ (rad) |
|---|---|---|---|---|---|---|---|---|---|---|
| Beyer et al. | TUA_Strong | 0.92 | 0.78 | 88.87 | 46.529 | 0.033 | 1.79E-03 | 0.40 | 0.173 | 4.52E-05 |
| | TUA_WeakPositive | 0.91 | 0.41 | 83.36 | 42.531 | 0.035 | 2.09E-03 | 0.40 | 0.169 | 5.72E-05 |
| | TUA_WeakNegative | 1.04 | 0.47 | 24.07 | 15.529 | 0.111 | 6.55E-04 | 0.75 | 0.326 | 5.56E-05 |
| | TUB_Strong | 0.98 | 0.99 | 76.29 | 38.726 | 0.038 | 1.55E-03 | 0.51 | 0.206 | 4.84E-05 |
| | TUB_WeakPositive | 0.95 | 0.48 | 68.55 | 34.797 | 0.042 | 1.73E-03 | 0.46 | 0.189 | 6.93E-05 |
| | TUB_WeakNegative | 1.03 | 0.57 | 12.84 | 7.598 | 0.189 | 3.78E-04 | 1.05 | 0.383 | 8.74E-05 |
| Ile and Reynouard | IleX_Strong | 1.11 | 0.68 | 26.86 | 13.297 | 0.100 | 4.94E-04 | 0.67 | 0.249 | 5.65E-05 |
| | IleY_WeakPositive | 1.13 | 0.45 | 25.72 | 11.431 | 0.104 | 5.81E-04 | 0.68 | 0.232 | 6.73E-05 |
| | IleY_WeakNegative | 1.11 | 0.50 | 9.18 | 4.613 | 0.246 | 2.25E-04 | 1.22 | 0.380 | 8.17E-05 |
| | IleXY_Strong | 1.05 | 0.65 | 24.51 | 11.956 | 0.109 | 4.65E-04 | 0.70 | 0.255 | 5.72E-05 |
| | IleXY_WeakPositive | 1.08 | 0.44 | 23.34 | 10.327 | 0.114 | 5.54E-04 | 0.71 | 0.239 | 6.80E-05 |
| | IleXY_WeakNegative | 0.83 | 0.37 | 8.15 | 4.137 | 0.269 | 2.14E-04 | 1.28 | 0.394 | 8.25E-05 |
| Lowes et al. | CW6_Strong | 1.00 | 0.43 | 74.45 | 40.027 | 0.039 | 6.45E-04 | 0.57 | 0.235 | 2.02E-05 |
| | CW7_Strong | 0.97 | 0.41 | 77.24 | 41.751 | 0.037 | 6.69E-04 | 0.55 | 0.229 | 2.00E-05 |
| | CW7_WeakPositive | 1.01 | 0.06 | 67.08 | 36.656 | 0.043 | 1.46E-03 | 0.34 | 0.157 | 4.70E-05 |
| | CW7_WeakNegative | 1.03 | 0.10 | 6.42 | 3.508 | 0.318 | 1.96E-04 | 1.45 | 0.442 | 6.84E-05 |
| | CW8_Strong | 0.95 | 0.41 | 76.09 | 41.353 | 0.038 | 6.59E-04 | 0.56 | 0.233 | 2.00E-05 |
| Brueggen | NTW1_WebPositive | 1.12 | 0.69 | 8.15 | 4.075 | 0.269 | 1.24E-04 | 1.46 | 0.422 | 3.85E-05 |
| | NTW1_WebNegative | 0.92 | 0.36 | 111.3 | 57.412 | 0.026 | 1.27E-03 | 0.31 | 0.138 | 2.50E-05 |
| | NTW1_Flange | 0.97 | 0.63 | 6.20 | 3.316 | 0.326 | 1.28E-04 | 1.27 | 0.404 | 4.36E-05 |
| | NTW2_WebPositive | 1.19 | 0.74 | 7.39 | 3.469 | 0.289 | 1.15E-04 | 1.53 | 0.418 | 4.07E-05 |
| | NTW2_WebNegative | 0.98 | 0.41 | 98.91 | 48.724 | 0.029 | 1.13E-03 | 0.33 | 0.140 | 2.62E-05 |
| | NTW2_Flange | 1.04 | 0.58 | 5.99 | 3.169 | 0.334 | 1.25E-04 | 1.24 | 0.396 | 4.36E-05 |
| Oesterle et al. | F1_Strong | 0.99 | 1.02 | 76.19 | 34.475 | 0.038 | 1.06E-03 | 0.57 | 0.205 | 3.71E-05 |
| | F2_Strong | 1.03 | 1.19 | 53.25 | 26.894 | 0.053 | 7.50E-04 | 0.75 | 0.275 | 3.65E-05 |
| Thomsen and Wallace | TW1_WebPositive | 0.74 | 0.86 | 4.37 | 2.441 | 0.407 | 1.54E-04 | 1.80 | 0.501 | 7.48E-05 |
| | TW1_WebNegative | 0.99 | 0.58 | 81.82 | 47.570 | 0.035 | 1.77E-03 | 0.38 | 0.181 | 4.36E-05 |
| | TW2_WebPositive | 0.94 | 0.89 | 3.85 | 2.127 | 0.438 | 1.43E-04 | 1.88 | 0.509 | 7.69E-05 |
| | TW2_WebNegative | 0.97 | 0.46 | 77.97 | 50.630 | 0.037 | 1.69E-03 | 0.36 | 0.189 | 3.96E-05 |
| Inada | L00A_FlangePositive | 0.61 | 3.82 | 13.61 | 8.147 | 0.181 | 3.56E-04 | 1.45 | 0.465 | 6.69E-05 |
| | L00A_FlangeNegative | 0.59 | 4.00 | 0.38 | -- | 0.888 | 7.11E-05 | 2.41 | -- | -- |
| | L45A_CornerPositive | 0.80 | 3.17 | 2.85 | 1.468 | 0.513 | 1.52E-04 | 2.35 | 0.548 | 1.12E-04 |
| | L45A_CornerNegative | 0.56 | 2.11 | 3.23 | 1.848 | 0.482 | 1.63E-04 | 2.07 | 0.542 | 1.00E-04 |
| Kono | L45C_CornerPositive | 2.04 | 1.35 | 1.58 | 0.516 | 0.655 | 2.08E-04 | 5.02 | -- | -- |
| | L45C_CornerNegative | 1.56 | 1.05 | 1.73 | 0.510 | 0.634 | 2.16E-04 | 3.45 | 0.504 | 3.10E-04 |
| | L45D_CornerPositive | 2.16 | 1.35 | 0.80 | -- | 0.789 | 1.73E-04 | 5.10 | -- | -- |
| | L45D_CornerNegative | 1.14 | 0.76 | 0.89 | 0.263 | 0.771 | 1.75E-04 | 3.67 | 0.521 | 3.20E-04 |
| Funaki | L1_CornerPositive | 1.75 | 2.54 | 1.56 | 0.775 | 0.658 | 2.11E-04 | 2.40 | 0.545 | 2.04E-04 |
| | L1_CornerNegative | 0.91 | 1.36 | 1.70 | 0.949 | 0.638 | 2.18E-04 | 2.11 | 0.541 | 1.81E-04 |
| | L2_CornerPositive | 1.63 | 2.27 | 1.45 | 2.037 | 0.674 | 2.06E-04 | 2.26 | 0.761 | 1.37E-04 |
| | L2_CornerNegative | 0.82 | 1.18 | 1.58 | 1.079 | 0.655 | 2.11E-04 | 1.95 | 0.571 | 1.58E-04 |
| | L5_CornerPositive | 1.50 | 2.67 | 0.87 | -- | 0.775 | 1.80E-04 | 2.44 | -- | -- |
| | L5_CornerNegative | 0.90 | 1.96 | 1.24 | 1.872 | 0.708 | 1.96E-04 | 2.45 | 0.788 | 1.44E-04 |
| | L6_CornerPositive | 1.45 | 2.88 | 1.31 | -- | 0.696 | 2.01E-04 | 2.46 | -- | -- |
| | L6_CornerNegative | 0.92 | 2.14 | 1.67 | 0.856 | 0.642 | 2.16E-04 | 2.32 | 0.544 | 1.98E-04 |
| Li | DL1_FlangePositive | 1.66 | 1.92 | 13.22 | 9.376 | 0.185 | 8.59E-04 | 0.97 | 0.408 | 1.26E-04 |
| | DL1_FlangeNegative | 1.41 | 1.78 | 0.77 | -- | 0.796 | 2.01E-04 | 1.76 | -- | -- |
| | DL2_FlangePositive | 1.56 | 2.00 | 10.37 | 8.230 | 0.224 | 7.09E-04 | 1.19 | 0.486 | 1.38E-04 |
| | DL2_FlangeNegative | 1.96 | 2.32 | 0.34 | -- | 0.898 | 1.75E-04 | 1.75 | -- | -- |
| | DL3_FlangePositive | 1.13 | 1.98 | 22.49 | 16.297 | 0.118 | 1.03E-03 | 0.70 | 0.337 | 8.38E-05 |
| | DL3_FlangeNegative | 0.99 | 2.28 | 1.29 | -- | 0.699 | 1.73E-04 | 1.75 | -- | -- |
| | DL4_FlangePositive | 1.05 | 1.54 | 29.33 | 21.254 | 0.093 | 1.30E-03 | 0.49 | 0.262 | 7.53E-05 |
| | DL4_FlangeNegative | 0.73 | 1.66 | 2.08 | -- | 0.591 | 2.06E-04 | 1.77 | -- | -- |

Two methods for computing displacement ductility were considered. Both employed an elastic-perfectly-plastic model to represent the envelope to the load-displacement response of the wall specimen. Both are depicted in Figure 14. For both, the horizontal/plastic portion of the model is defined to be tangent to response envelope at the point of maximum load. The methods then differ in how the linear elastic portion of the model is defined. Using the first method (Figure 14(a)), the elastic stiffness is defined by the secant to the response envelope between the points of zero load and 75% of maximum experimental load. Using the second method (Figure 14(b)), the elastic portion of the model is defined by the line that results in zero energy error, that is the line for which the area above the line and below the response envelope is equal to the area below the line and above the response envelope. For the second method, an iterative approach was used to solve for slope of the line. The two methods were found to provide similar results, and both methods were found to predict yield displacements that were in good agreement with the experimentally yield displacement (defined as the measured displacement at which the computed yield moment was reached). Therefore, the 75% method was used due to its simplicity. Given the elastic-perfectly-plastic response model, ductility was computed as the displacement at 20% loss in lateral load carrying capacity divided by the displacement at which the maximum strength of the bilinear model is achieved (identified as point A in Figure 14(a)).

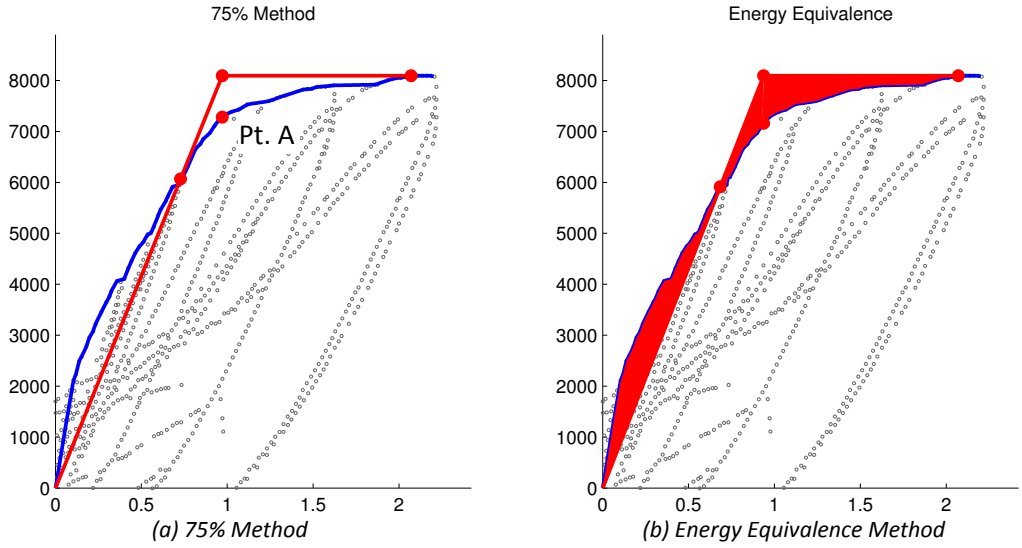


**Figure 14: Comparison of methods used to define the elastic-perfectly-plastic response model (red line) from the envelope to the experimental load-displacement history (blue line).**

## 5.2 Evaluation of Correlation between Design Parameters and Ductility

Displacement ductility was plotted versus each of the design parameters defined in Table 4, Table 5 and Table 6 with data grouped on the basis of wall shape, unidirectional versus bidirectional load history and failure mechanism under unidirectional and bidirectional loading. These plots are provided below for design parameters for which correlation was observed and for design parameters of particular interest to the study. These plots are compared with plots of drift capacity versus the parameter for planar walls and for ACI Code compliant walls from Birely (2012). Plots of ductility versus design parameter not provided below indicated that the following parameters were not significantly correlated with ductility: scale, $f_c'$, $\rho_v$, $\rho_h$, $V_n/\left(A_{cv}\sqrt{f_c'}\right)$, $M_u/M_n$, $\phi_y$, $c_{yield}/l_w$, $\varepsilon_t$, $c/l_w$.

### 5.2.1 Shear span ratio

Figure 15 shows deformation capacity versus shear span ratio, $M/(Vl_w)$. All but two of the walls examined in this study had shear span ratios between two and for. Two nonplanar walls had shear span ratios of 7; for nonplanar walls, larger shear span ratios correspond to weak-axis loading of T- and C-shaped walls. For ACI Code compliant planar walls, increasing aspect ratio resulted in increased drift capacity (Figure 15 (e)). Nonplanar walls subjected to unidirectional loading history show a weak correlation between ductility and shear span ratio, but with increasing shear span corresponding to reduced ductility in walls subjected to bidirectional loading. Ultimately, the data in Figure 15 are interpreted as shear span ratio having minimal impact on ductility. Correlation shown for planar walls may be attributed to walls with larger shear span ratios being more flexible and, thus, exhibiting larger drift capacities. Correlation for nonplanar walls may be attributed to bidirectional walls exhibiting reduced deformation capacity in comparison with unidirectionally loaded walls.

### 5.2.2 Axial load ratio

Figure 16 shows deformation capacity versus axial load ratio, $\lambda_N$. The nonplanar walls examined in the study had axial load ratios ranging from 2% to 30%; planar wall axial load ratios ranged from 0% to 13%. Both data sets suggest that increasing axial load ratio reduced deformation capacity and that walls with higher axial load ratios exhibit low ductility / drift capacity. The data show also that the tests with higher axial load ratios typically exhibit a crushing-buckling failure mechanism. Nearly all of the walls exhibiting crushing-buckling failures had axial load ratios of 1%f'cAg or greater and ductility ratios less than five. The two outlying CB failures were T-shaped walls subjected to a bi-directional loading history.

### 5.2.3 Boundary element longitidinal reinforcement ratio

Figure 17 shows deformation capacity versus boundary element longitudinal reinforcement ratio, $\rho_{be}$. For nonplanar walls, a strong correlation between boundary element reinforcing and ductility can be observed, with larger reinforcement ratios resulting in reduced drift capacity and increased likelihood of compression-controlled failure. This trend can be explained by a larger boundary element reinforcement ratio resulting in a larger tension force that must be equilibrated in the compression zone. Similar trends are not observed for planar walls;

### 5.2.4 Boundary element confining reinforcement ratio

Figure 18 shows deformation capacity versus boundary element volumetric confining reinforcement ratio, $\rho_{con}$. No correlation was observed between boundary element confining reinforcing ratio and ductility or drift capacity. T

### 5.2.5 Compressive strain at yield:

Figure 19 shows deformation capacity versus concrete compressive strain at computed first yield of reinforcing steel, $\varepsilon_c$. Both planar and nonplanar wall data show that increasing magnitude in concrete compressive strain is weakly correlated with decreasing deformation capacity. Both planar and nonplanar wall data show compression-controlled failure is more likely if the magnitude of the concrete compression strain at yield is larger, while buckling-rupture failure is more likely if the magnitude of the concrete compressive strain at yield is smaller.

### 5.2.6 Tensile strain at nominal:

Figure 20 shows deformation capacity versus the tensile strain in the extreme longitudinal reinforcing bar at nominal flexural strength normalized by yield strain, $\varepsilon_t/\varepsilon_y$. The ACI Code classifies flexural elements with $\varepsilon_t > 0.005$ as tension-controlled ($\varepsilon_t/\varepsilon_y$ > 2.4 for Grade 60 steel). For nonplanar walls, normalized steel strain ranges from 2 to 58; for planar walls the range is 3 to 24. The data do not show

deformation capacity to be correlated with normalized steel strain demand at nominal flexural strength. However, for all ACI Code compliant planar walls and most nonplanar walls, compression-controlled flexural failures are observed for walls with $\varepsilon_t/\varepsilon_y$ < 10 with tension-controlled buckling-rupture failures observed for ($\varepsilon_t/\varepsilon_y$ > 10) two L-shaped walls with $\varepsilon_t/\varepsilon_y$ < ~20 exhibit compression-controlled failure). This indicates that the ACI criterion for establishing tension-controlled flexural response is too low for walls, and that $\varepsilon_t > 0.02$ would be a better limit for walls.

### 5.2.7 Nominal curvature

Figure 21 shows deformation capacity versus curvature at nominal flexural strength, $\phi_n$. When the entire planar wall data set is considered, there is no correlation between curvature at nominal strength and drift capacity. However, if only ACI Code compliant planar walls are considered, the data show increasing curvature at nominal results in increased drift capacity; removing non-Code compliant walls from the data set removes a number of walls with low drift capacities and high curvatures. For nonplanar walls, there is no significant correlation between curvature at nominal and ductility; with the exception of three U-shaped wall data points that represent high ductility and large curvature, the remainder of the data are randomly distributed over the design space. Additional research is required to determine why trends observed for Code compliant planar walls do not extend to nonplanar walls.

### 5.2.8 Summary and conclusions regarding correlation between design parameters and ductility for planar and nonplanar walls

The impact of 18 design parameters on deformation capacity was investigated for planar and nonplanar walls; deformation capacity was defined by drift capacity for planar walls and displacement ductility for nonplanar walls. The results of this investigation show no significant correlation between deformation capacity and the following parameters: specimen scale, shear span ratio( $M/(Vl_w)$), concrete compressive strength ($f_c'$), gross longitudinal reinforcement ratio ($\rho_{total}$), horizontal reinforcement ratio ($\rho_h$), boundary element confining reinforcement ratio ($\rho_{con}$), shear stress demand $\left(V_n/\left(A_{cv}\sqrt{f_c'}\right)\right)$, flexural over-strength $(M_u/M_n)$, yield curvature $\left(\phi_y\right)$, ratio of neutral axis depth at yield to wall length$\left(c_{yield}/l_w\right)$, steel strain at nominal strength($\varepsilon_t$), ratio of neutral axis depth at nominal to wall length $(c/l_w)$.

The following design parameters were found to correlate with deformation capacity and/or failure mechanism:

- Axial load ratio: Deformation capacity decreases with increasing axial load ratio and walls with higher axial load ratios typically exhibit compression-controlled failure.
- Concrete compressive strain at yield: Deformation capacity decreases with decreasing concrete compression strain at first yield of tension steel; this trend is stronger for nonplanar walls than for planar walls. For all walls, crushing-buckling failure is more likely if compression strains at yield are large in magnitude while buckling-rupture failure is more likely if compression strains at yield are small in magnitude.
- Normalized steel tension strain at nominal flexural strength: Deformation capacity is not correlated with normalized steel tension strain at nominal flexural strength $\left(\varepsilon_t/\varepsilon_y\right)$. However, for walls not susceptible to shear failure, crushing-buckling failure is likely to occur if $\varepsilon_t/\varepsilon_y < 10$, while buckling-rupture failure occurs is likely to occur if $\varepsilon_t/\varepsilon_y > 10$.

Additionally, the following design parameters were found to impact the deformation capacity and/or failure mechanism of either planar *or* nonplanar walls, but not both. As such, further research is required to understand the mechanism by which these parameters affect behavior:

- Boundary element longitudinal reinforcement ratio: For nonplanar walls, ductility decreases and the likelihood of a compression-controlled failure increases with increasing boundary element reinforcement ratio. This is attributed to increased reinforcement producing, under flexural loading, increased tension that must be equilibrated by compression zone concrete and steel; thus, increased reinforcing steel results in increased compression demand, increased likelihood of compression-controlled failure and reduced ductility. Similar behavior and trends could be expected for planar walls; however, boundary element reinforcement ratio has no significant impact on the behavior of planar walls. Thus, further research is required.
- Curvature at nominal flexural strength: For ACI Code compliant planar walls, increased curvature at nominal flexural strength is correlated with increased drift capacity. For nonplanar walls, there is no significant correlation, though there are three U-shaped wall data points with high curvatures at nominal strength do exhibit high ductility.

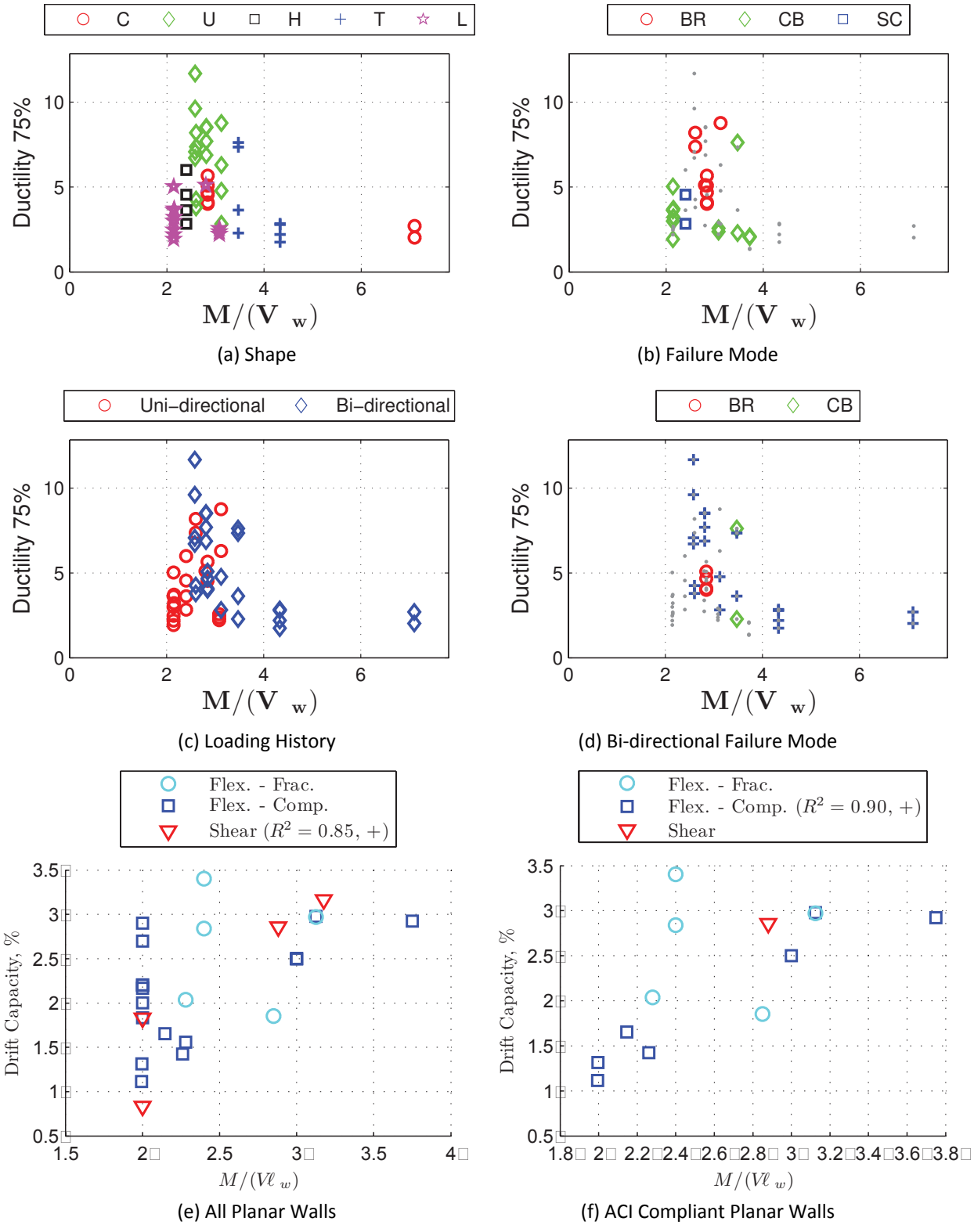


**Figure 15: Ductility and drift capacity versus shear span ratio**

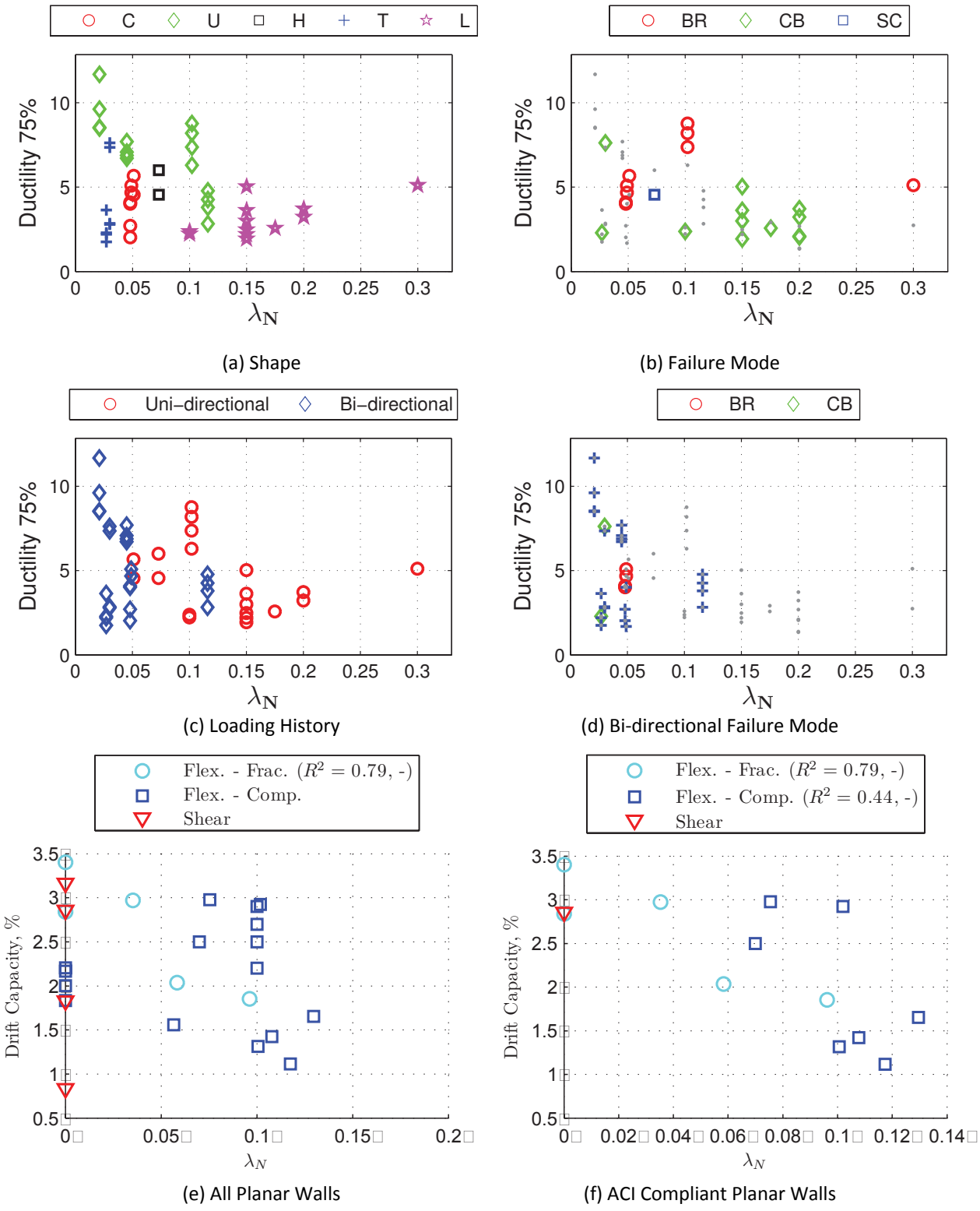


(a) Shape

(b) Failure Mode

(c) Loading History

(d) Bi-directional Failure Mode

(e) All Planar Walls

(f) ACI Compliant Planar Walls

**Figure 16: Ductility and drift capacity versus axial load ratio**

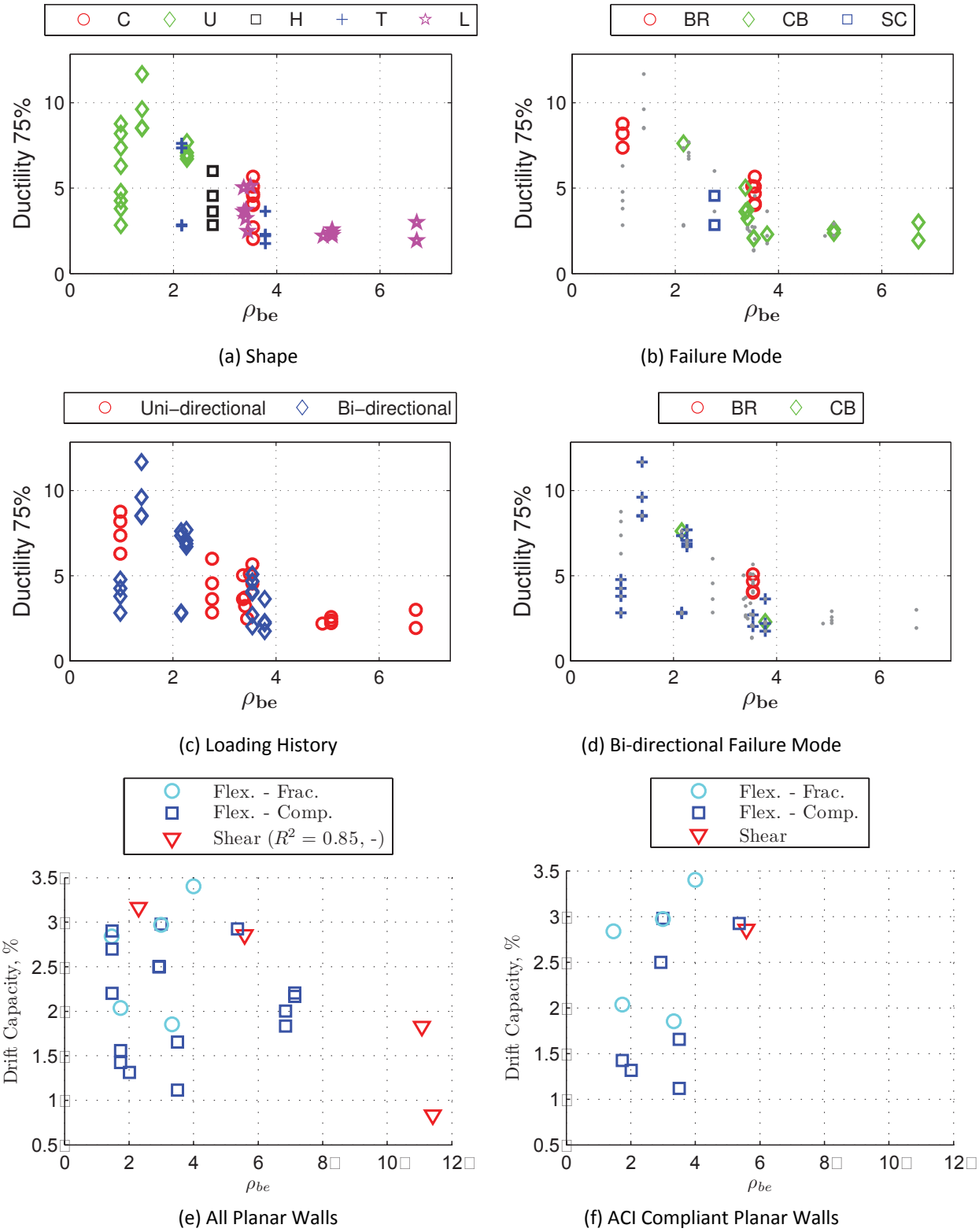


**Figure 17: Ductility and drift capacity versus boundary element longitudinal reinforcement ratio**

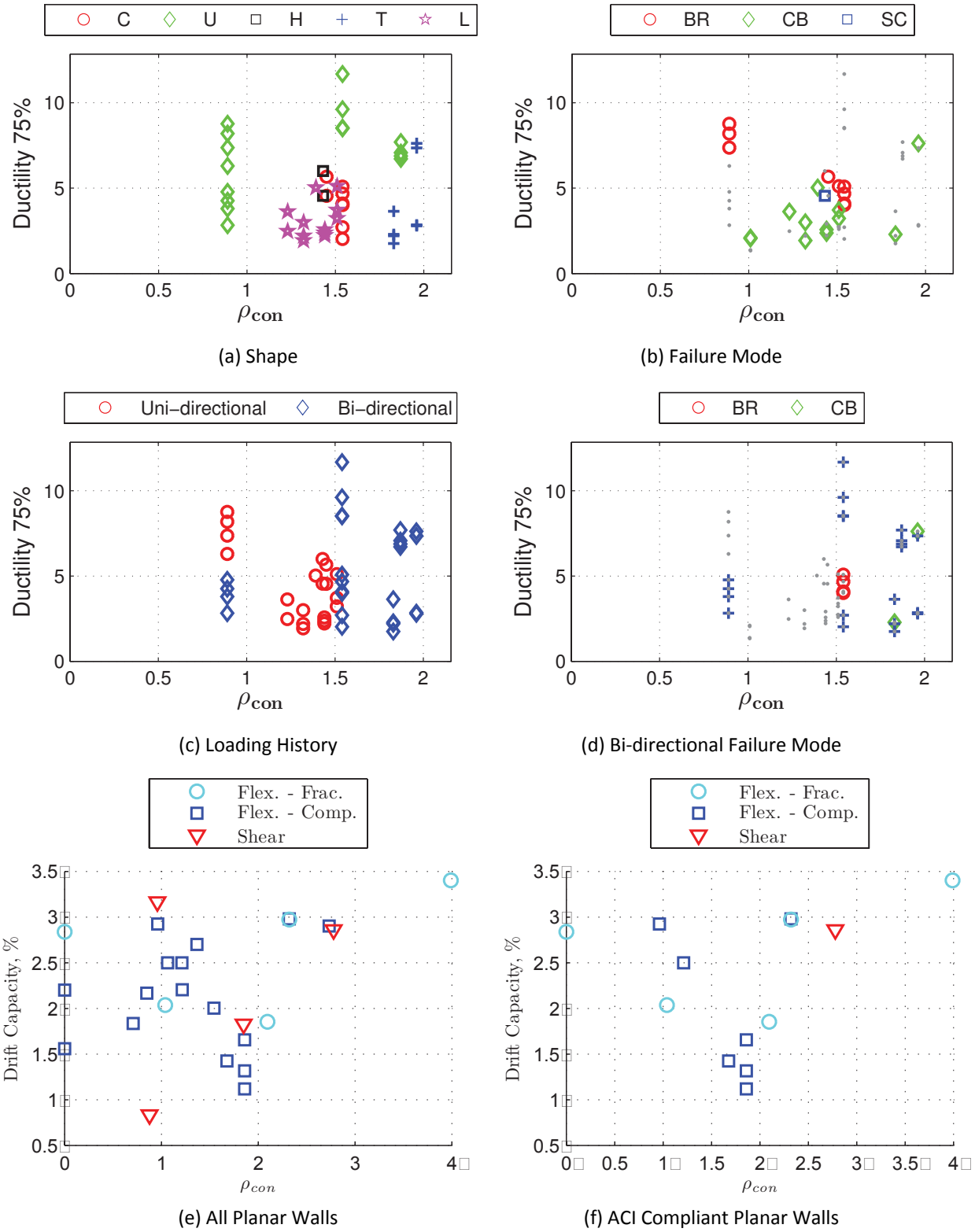


(a) Shape

(b) Failure Mode

(c) Loading History

(d) Bi-directional Failure Mode

(e) All Planar Walls

(f) ACI Compliant Planar Walls

**Figure 18: Ductility and drift capacity versus volumetric reinforcing ratio**

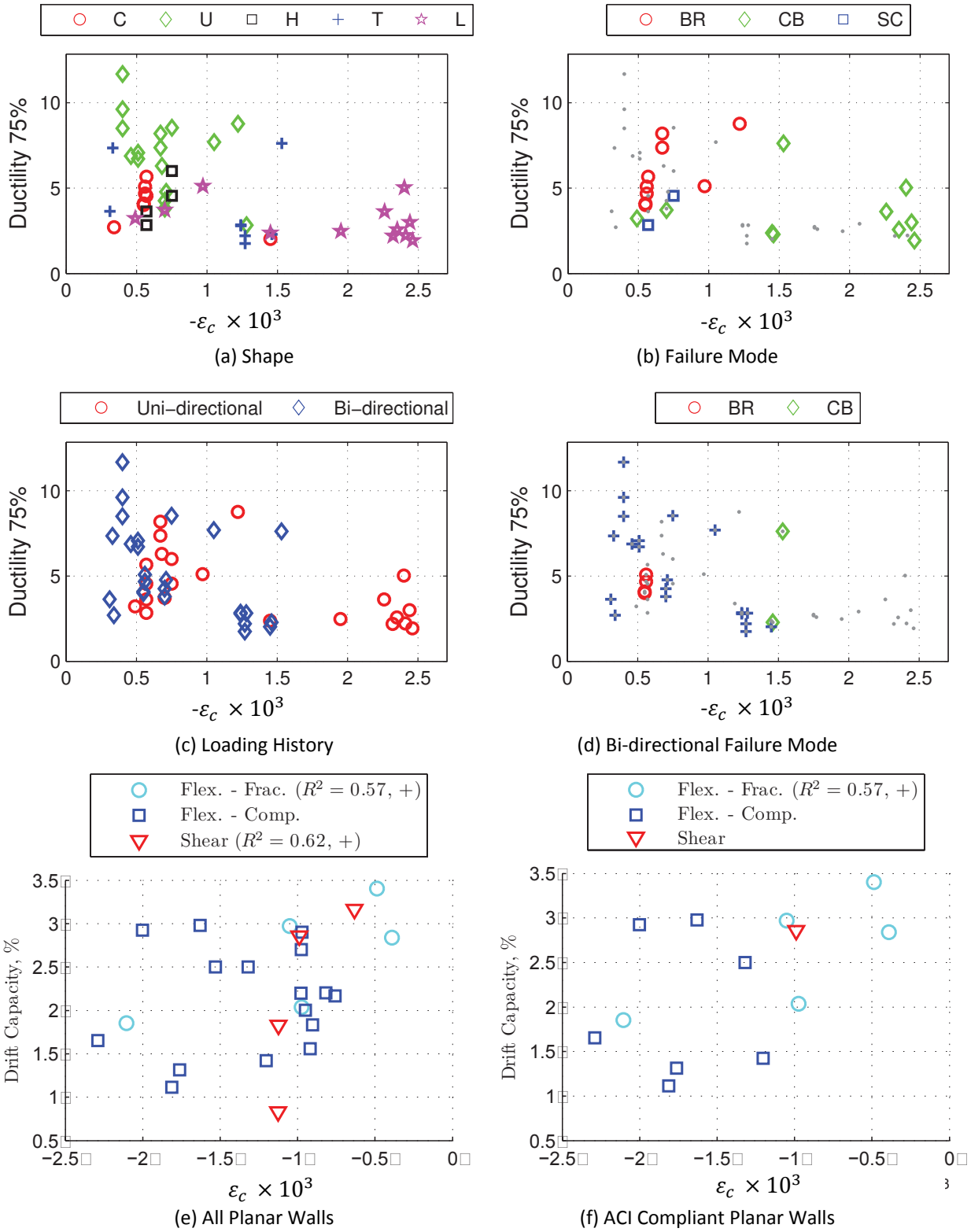


**Figure 19: Compressive strain at yield**

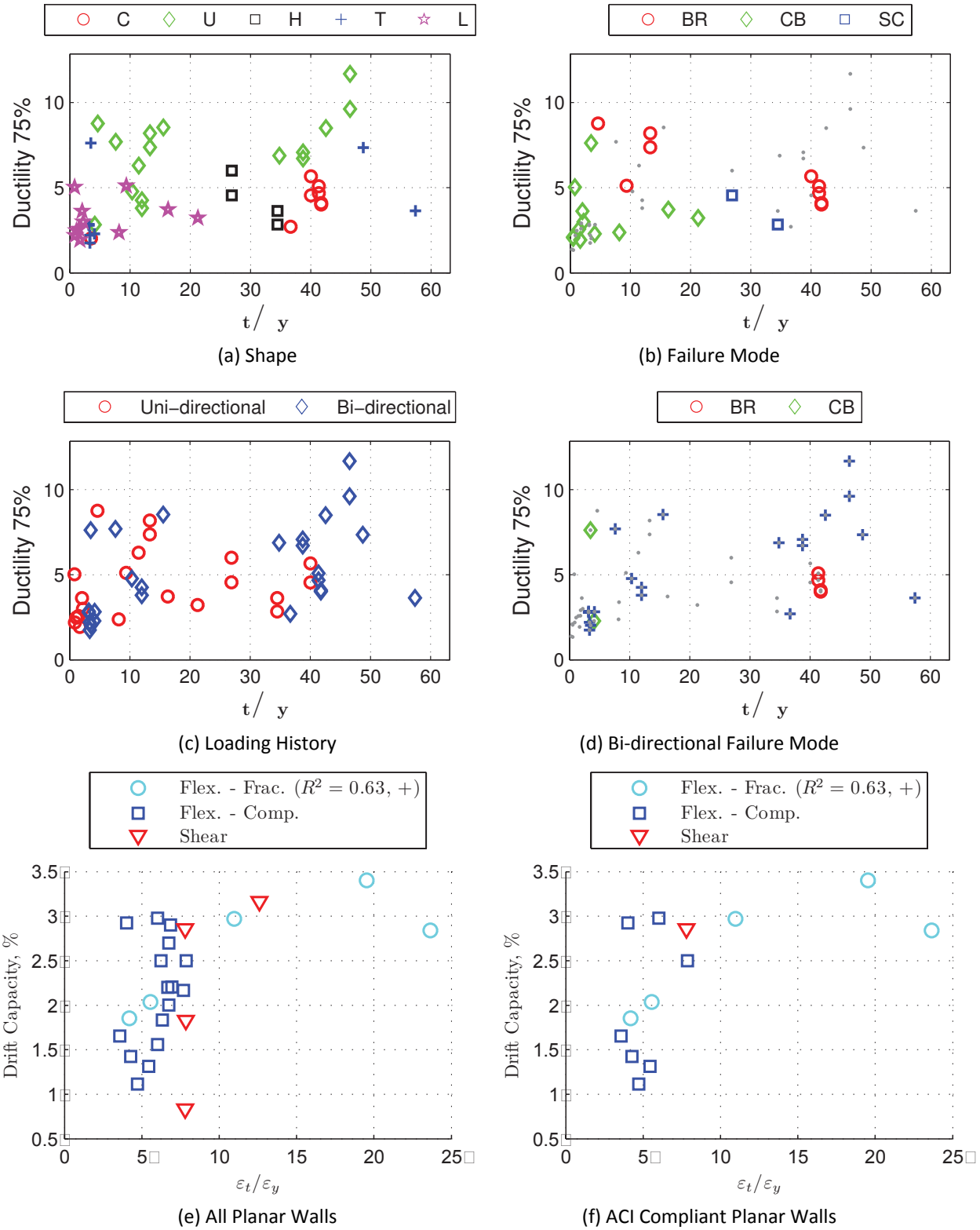


**Figure 20: Normalized tensile strain**

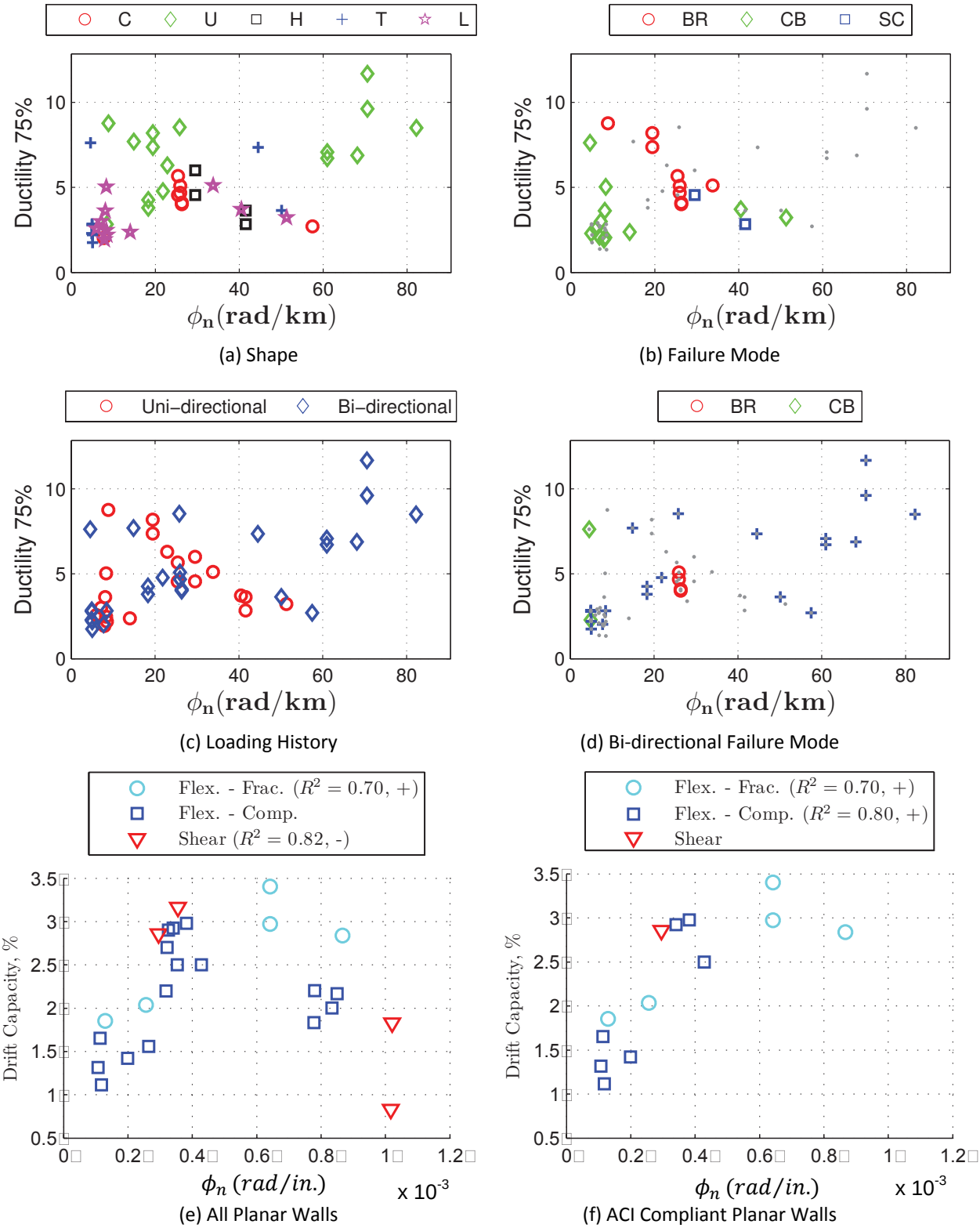


**Figure 21: Nominal curvature**

# 6 OBSERVATIONS AND CONCLUSIONS ABOUT THE BEHAVIOR OF NONPLANAR WALLS

The above experimental investigations support a number of significant observations and conclusions about the behavior of nonplanar walls subjected to cyclic lateral loading. These observations and conclusions, which are listed below, have implications for analysis and design. Unfortunately, in many cases, observations suggest that further research is required to fully understand the mechanisms that determine nonplanar wall behavior and advance analysis and design.

- Deformation capacity: well-detailed nonplanar concrete walls subjected to bidirectional displacement histories can maintain strength and stiffness to large displacement ductilities (>6) and drift demand levels (>2% story drift). However, this requires that the wall meet design criteria that reduce the likelihood of severe local compression demands under general loading; this is not currently directly addressed by the ACI Code. For all walls, data show that deformation capacity increases with reduction in axial load and reduction in concrete compressive strain at first yield of reinforcing steel. For nonplanar walls, data show that deformation capacity is enhanced also by reduction in boundary element reinforcement ratio and the expansion of confined concrete regions.
- Potential for compression-controlled response: compression-controlled failure characterized by simultaneous buckling of reinforcing steel and concrete crushing is typically associated with reduced deformation capacity and rapid strength loss. The potential for compression-controlled failure increases with increased axial load, increased concrete compression strain at yield, increased boundary element longitudinal reinforcement ratio, and steel strain at nominal flexural stress less than $10\varepsilon_y$. The data considered as part of this study suggest that the volume of boundary element confining reinforcement has no impact on the potential for compression-controlled failure.
- Impact of wall configuration on performance. Data show that nonplanar wall configurations can enhance performance by reducing compression demands and improving stability. For example, comparing an H-shaped wall and a T-shaped wall, compression demands in the tip of the stem of the T-shaped wall would be substantially reduced in the H-shaped wall; this would reduce the likelihood of a compression-controlled failure and for out-of-plane instability failure. However, nonplanar wall configurations and general lateral load histories offer the potential for severe local compression demands that can accelerate the onset of damage, expand the damaged region of the wall and lead to reduced deformation capacity. This results from general loading activating a large volume of longitudinal reinforcement in tension and a relatively small region of reinforced concrete in compression. The potential for severe local compression demands to impair performance can be evaluated using design parameters discussed above.
- Impact of bidirectional loading on wall performance: Two experimental investigations compare nominally identical walls subjected to unidirectional and bidirectional lateral load patters; data from these investigations suggest that bidirectional loading does not reduce strength but does reduce deformation capacity. When walls subjected to both unidirectional and bidirectional lateral load histories are considered, the data suggest that the lateral load pattern has no impact on deformation capacity or failure mode.
- Shear transfer in nonplanar walls: Data suggest that shear transfer in nonplanar walls is complex. Because shear is transferred through compression struts that develop in compression regions and because compression regions may be small in nonplanar walls subjected to bidirectional lateral loading, shear can result in crushing of the unconfined web region of the

wall, “framing-action” in which shear results in out-of-plane bending of wall boundary elements or flanges, and sliding shear failure of the web region of the wall. Further research is required to advance understanding of shear design for nonplanar walls.

- Numerical modeling of walls: Data show that vertical strain distributions on wall cross sections are not linear, as is assumed by i) the ACI Code for calculation of wall flexural strength and ii) most fiber-type section analysis software packages for calculation of the moment-curvature response of the cross section. However, force-based beam-column elements that employ fiber-type section models have been shown to provide accurate simulation of wall specimen response for unidirectional and bidirectional loading. Thus, additional research is required to determine the conditions under which fiber-type section analyses can and cannot be used to simulate wall response.

## 7 ACKNOWLEDGEMENTS

The research presented herein was funded by the Charles Pankow Foundation and the National Science Foundation through the Network for Earthquake Engineering Simulation Research Program, Grant CMS-042157, Joy Pauschke, program manager. Any opinions, findings, and conclusions or recommendations expressed in this material are those of the authors and do not necessarily reflect the views of the Charles Pankow Foundation or the National Science Foundation.

## 8 REFERENCES

Beyer K, Dazio A, Priestley MJN (2008). “Quasi-Static Cyclic Tests of Two U-Shaped Reinforced Concrete Walls,” *Journal of Earthquake Engineering* 12:7, 1023-1053.

Birely AC (2012). “Seismic Performance of Slender Reinforced Concrete Structural Walls,” *PhD Dissertation,* University of Washington, 983p.

Brueggen BL (2009). “Performance of T-shaped Reinforced Concrete Structural Walls under Multi-Directional Loading,” *PhD Dissertation*, University of Minnesota.

Hosaka G, Funaki H, Hosoya H, Imai H (2008). “Experimental Study of Structural Performance of RC Shear Wall with L-shaped Section,” *Proceedings of the 14$^{th}$ World Conference on Earthquake Engineering October 12-17, 2008, Beijing, China*.

Ile N, Reynouard JM (2005). “Behavior of U-Shaped Walls Subjected to Uniaxial and Biaxial Cyclic Lateral Loading,” Journal of Earthquake Engineering 9:1, 67-94.

Inada K, Chosa K, Sato H, Kono S, Watanabe F (2008). “Seismic Performance of RC L-shaped Core Structural Walls,” *Proceedings of the 14$^{th}$ World Conference on Earthquake Engineering October 12-17, 2008, Beijing, China*.

Kono S, Sakamoto K, Sakashita M (2011). “Simulation of Seismic Load Resistance of Core-Walls for Tall Buildings,” *Applied Mechanics and Materials* 82: 386-391.

Li W, Li QN (2012). “Seismic Performance of L-shaped RC Shear Wall Subjected to Cyclic Loading,” *The Structural Design of Tall and Special Buildings* 21: 855-866.

Lowes LN, Lehman DE, Kucham DA, Behroozi A, Mock A (2014). “Large Scale Testing of C-Shaped Reinforced Concrete Walls,” A Report to the Charles Pankow Foundation on Grant , 78p.

Oesterle RG, Fiorato AE, Johal LS, Carpenter JE, Russell HG, Corely WG (1976). “Earthquake Resistant Structural Walls – Tests of Isolated Walls” *Report to the National Science Foundation for Grant No. GI-43880*. PCI, Skokie, IL.

Oesterle RG, Aristizabal-Ochoa JD, Fiorato AE, Russell HG, Corely WG (1979). “Earthquake Resistant Structural Walls – Tests of Isolated Walls – Phase II” *Report to the National Science Foundation for Grant No. ENV77-15333*. PCI, Skokie, IL.

Paulay T, Goodsir WJ (1985). “The Ductility of Structural Walls,” Belletin of the New Zealand National Society for EArhtquake Engineering (18)3: 250-269.

Pegon, P, Plumier C, Pinto A, Molina J, Gonzalez P, Tognoli P C, Hubert O (2000). "U-shaped walls: Description of the experimental set-up," *TMR-ICONS*-TOPIC5, JRC Ispra, April, 23p.

Pegon, P, Plumier C, Pinto A, Molina J, Gonzalez P, Tognoli P C, Hubert O (2000). "U-shaped walls: quasi-static test in the Y-direction," *TMR-ICONS*-TOPIC5, JRC Ispra, May, 19p.

Pegon, P, Plumier C, Pinto A, Molina J, Gonzalez P, Tognoli P C, Hubert O (2000). "U-shaped walls: quasi-static test in the X-direction," *TMR-ICONS*-TOPIC5, JRC Ispra, June, 23p.

Pegon, P, Plumier C, Pinto A, Molina J, Gonzalez P, Tognoli P C, Hubert O (2000). "U-shaped walls: quasi-static test in the X- and Y-directions," *TMR-ICONS*-TOPIC5, JRC Ispra, June, 23p.

Reynouard JM, Fardis MN (2001). "Shear wall structures," *Cafeel-Ecoest Thematic Report No. 5, Eds.* RT Severn and R Bairrao, September, 240 p.

Thomsen JH, Wallace JW (1995). “Displacement-Based Design of Reinforced Concrete Structural Walls: An Experimental Investigation of Walls with Rectangular and T-shaped Cross-Sections,” *A Report to the National Science Foundation on Grant No. NSF-BCS-9112962*. June, 375p.